MgO-based Magnetic Tunnel Junctions Doped With Paramagnetic Impurities: Towards Quantum Energy Harvesting

Maria Barbosa Grácio
Mestrado em Engenharia Física
Departamento de Física e Astronomia
2022

Orientador
Prof. Dr. Ricardo Ferreira, INL

Coorientador
Prof. Dr. João Ventura, IFIMUP/FCUP

U.PORTO

FACULDADE DE CIÊNCIAS
UNIVERSIDADE DO PORTO

Todas as correções determinadas pelo júri, e só essas, foram efetuadas.

O Presidente do Júri,

Porto, _____/_____/_____

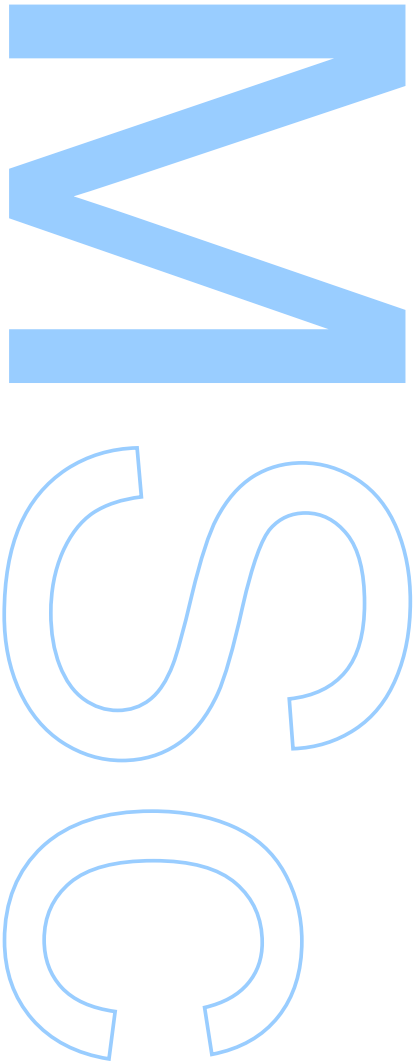

UNIVERSIDADE DO PORTO

MASTERS THESIS

MgO-based Magnetic Tunnel Junctions Doped With Paramagnetic Impurities: Towards Quantum Energy Harvesting

Author:
Maria BARBOSA GRÁCIO

Supervisor:
Ricardo FERREIRA

A thesis submitted in fulfilment of the requirements
for the degree of MSc. Engineering Physics

at the

Faculdade de Ciências da Universidade do Porto
Departamento de Física e Astronomia

January 5, 2023

Sworn Statement

I, Maria Barbosa Grácio, enrolled in the Master Degree Engineering Physics at the Faculty of Sciences of the University of Porto hereby declare, in accordance with the provisions of paragraph a) of Article 14 of the Code of Ethical Conduct of the University of Porto, that the content of this dissertation reflects perspectives, research work and my own interpretations at the time of its submission.

By submitting this dissertation, I also declare that it contains the results of my own research work and contributions that have not been previously submitted to this or any other institution.

I further declare that all references to other authors fully comply with the rules of attribution and are referenced in the text by citation and identified in the bibliographic references section. This dissertation does not include any content whose reproduction is protected by copyright laws.

I am aware that the practice of plagiarism and self-plagiarism constitute a form of academic offense.

Maria Barbosa Grácio

Porto, October 28, 2022

Agradecimentos

Quero agradecer em primeiro lugar ao meu orientador João Ventura, por todo o tempo que dedicou ao meu trabalho, pela sua paciência, sabedoria e orientação. Agradeço também por me ajudar sempre a ver o lado positivo daquilo que tantas vezes me pareceu não ter solução e pela sua capacidade de simplificar todos os problemas.

Agradeço ao meu orientador Ricardo Ferreira, pela oportunidade de trabalhar neste tema e pelo seu entusiasmo com o trabalhado desenvolvido.

Deixo também um agradecimento ao grupo de Spintrónica do INL, especialmente à Elvira Paz, pela sua colaboração, sem a qual este trabalho não teria sido desenvolvido, e à Luana Benetti e Alejandro Schulman, por tão clara e pacientemente me mostrarem o funcionamento da sala limpa e das técnicas de fabricação de junções de túnel. Agradeço ao João Silva, pela sua colaboração ao longo das nossas dissertações, e a todos os investigadores do grupo do IFIMUP, que de uma ou outra forma ajudaram com as minhas dúvidas de iniciante.

Aos amigos que me acompanharam ao longo dos anos de faculdade, agradeço muito a sua amizade e apoio, e por arranjarem sempre uma forma de me fazer rir nos momentos mais stressantes.

Aos amigos que me acompanham ao longo da vida e à minha família, agradeço por, mesmo quando não nos vemos com a regularidade desejada, continuarem sempre presentes na minha vida.

Um agradecimento muito especial ao João Manuel Pinho, por acreditar em mim incondicionalmente, por me deixar sempre tão orgulhosa e me inspirar a fazer melhor, e por ser o melhor amigo que alguma vez poderia pedir.

Finalmente, agradeço aos meus pais por me terem proporcionado todas as oportunidades, por me darem sempre todo o seu apoio em todos os aspetos da minha vida, e por verem sempre o melhor de mim.

UNIVERSIDADE DO PORTO

Abstract

Faculdade de Ciências da Universidade do Porto
Departamento de Física e Astronomia

MSc. Engineering Physics

MgO-based Magnetic Tunnel Junctions Doped With Paramagnetic Impurities: Towards Quantum Energy Harvesting

by Maria BARBOSA GRÁCIO

The growing interest in Spintronics led to the development of magnetic tunnel junctions (MTJs), a device which presents tunnelling magnetoresistance (TMR). This device is composed of two ferromagnetic (FM) layers separated by a nanometric insulator material, which enables an electrical current to flow through quantum tunnelling. It has great application in sensors and magnetic memories, namely the prominent magnetoresistive random access memory (MRAM). In recent years, with the growing need for larger data storage capability and higher data processing speed, a new application branch on spin-assisted energy harvesting has emerged. This thesis will follow a recent path reporting the use of MgO-based MTJs to harvest thermal fluctuations of paramagnetic centres. Towards this objective, we fabricated and characterized MTJs with tantalum-doped MgO tunnel barriers, deposited using magnetron sputtering. The fabrication of the devices was performed at the International Iberian Nanotechnology Laboratory (INL), and the characterization and transport measurements were performed at the Instituto de Física de Materiais Avançados, Nanotecnologia e Fotónica da Universidade do Porto (IFIMUP) facilities. To understand the main consequences of the introduction of the Ta particles, measurements of TMR and current-voltage characteristics were performed both in Ta-doped samples and also in similar control junctions. TMR values of 163% and 73% were obtained for control and Ta-doped samples, respectively, measured at room temperature. We concluded that the Ta particles cause an increase of the MTJ resistance, more prominently in the parallel state, due to the increase in the effective thickness of the barrier. At the same time, as impurities in the tunnel barrier, they open extra impurity assisted conductance channels for electrons, originating a relevant decrease in the TMR ratio, with a

strong dependency on temperature and the bias. This dependency is reflected by a ratio of TMR_{28K}/TMR_{300K} = 2.8 in Ta-doped junctions, and a figure of merit $V_{1/2}$ = 0.12 V at room temperature. Given the obtained results, no energy generation effect could be definitely confirmed in these junctions.

This work allowed to understand the impact of introducing paramagnetic particles in the tunnel barrier on the overall MTJ performance. As a perspective for the future, we aim to vary parameters, such as concentration/thickness of paramagnetic particles and tunnel barrier thickness, to perform a complete characterization and compare the results, towards the energy harvesting effect.

UNIVERSIDADE DO PORTO

Resumo

Faculdade de Ciências da Universidade do Porto
Departamento de Física e Astronomia

Mestrado em Engenharia Física

Junções Magnéticas de Efeito de Túnel com Barreira de MgO Dopada com Impurezas Paramagnéticas

por Maria BARBOSA GRÁCIO

O crescente interesse na área da Spintrónica levou ao desenvolvimento de junções magnéticas de túnel (MTJs), um dispositivo que apresenta magnetorresistência de túnel (TMR). Este dispositivo é composto por duas camadas ferromagnéticas separadas por um material isolador nanométrico, que permite com que a corrente elétrica seja transmitida por efeito de túnel. O dispositivo tem aplicação em sensores e memórias magnéticas, nomeadamente a proeminente random access memory magnetorresistiva (MRAM). Recentemente, dada a crescente necessidade de aumento da capacidade de armazenamento e velocidade de processamento de dados, surgiu um novo ramo de aplicação baseado na recolha de energia assistida por spin. Esta tese segue um caminho recente, em que é reportado o uso de junções magnéticas de túnel com barreira de MgO, para recolha das flutuações térmicas de centros paramagnéticos. De encontro a este objetivo, fabricámos e caracterizámos junções com barreira de túnel de MgO dopada com tântalo, depositadas através de pulverização catódica. Os dispositivos foram fabricados no International Iberian Nanotechnology Laboratory (INL), e a sua caracterização e medidas de transporte foram realizadas nas instalações do Instituto de Física de Materiais Avançados, Nanotecnologia e Fotónica da Universidade do Porto (IFIMUP). De modo a compreender as principais consequências da introdução de partículas de tântalo, medidas de TMR e características de corrente-tensão foram realizadas tanto nas amostras dopadas, como em amostras similares de controlo. Os valores de TMR obtidos em amostras medidas a temperatura ambiente foram de 163% e 73%, para uma amostra de controlo e uma dopada com tântalo, respetivamente. Concluímos que as partículas de Ta causam o aumento da

resistência das MTJs, mais relevante no estado paralelo de magnetização, devido ao aumento da espessura efetiva da barreira. Ao mesmo tempo, as partículas comportam-se como impurezas, abrindo caminhos de condução para os eletrões, o que leva à diminuição significativa do TMR, com elevada dependência na temperatura e tensão aplicadas. Esta dependência reflete-se na razão $TMR_{28K}/TMR_{300K} = 2.8$ nas junções dopadas com tântalo, e na figura de mérito $V_{1/2} = 0.12$ V a temperatura ambiente. Além disso, os resultados obtidos não permitem afirmar definitivamente que o efeito de geração de energia foi observado nas junções estudadas.

Este trabalho permitiu compreender o impacto da introdução de partículas paramagnéticas de tântalo na barreira de túnel na performance global das MTJs. Como perspetiva futura, pretendemos variar vários parâmetros, tais como concentração/espessura das partículas paramagnéticas e espessura da barreira de túnel, de modo a obter uma caracterização completa e realizar uma comparação de resultados, de encontro ao efeito de recolha de energia.

Contents

List of Figures

List of Tables

Glossary

MTJ	Magnetic Tunnel Junction
TMR	Tunnel Magnetoresistance
MR	Magnetoresistance
R	Resistance
GMR	Giant Magnetoresistance
MRAM	Magnetoresistive Random Access Memory
STT	Spin Transfer Torque
FM	Ferromagnetic
TB	Tunnel Barrier
P	Parallel
AP	Anti-parallel
DOS	Density of States
I	Insulator
EMF	Eletromotive Force
V	Voltage
T	Temperature

Chapter 1

Tunnelling Magnetoresistance: an Overview

1.1 Spintronics

Tunnelling magnetoresistance (TMR) is a phenomenon that was uncovered due to the growing interest in the area of Spintronics, which is a research and technological field that takes advantage on the spin of electrons, and not only on its charge, like conventional electronics. The main physical phenomenon in Spintronics is the magnetoresistive effect. Magnetoresistance (MR) is the property of a material to change its electrical resistance (R) under the application of an external magnetic field (H). This effect can be described, in a general way, as the relative difference between the resistance of a device under the application of a magnetic field, and no applied magnetic field:

$$MR = \frac{R(H) - R(0)}{R(0)} \ (\%). \tag{1.1}$$

The reasons behind this resistance variation can be various, leading to magnetoresistive effects with different origins. One of them is Anisotropic magnetoresistance (AMR), in which the resistance varies as a function of the angle between the magnetization and the direction of the current flowing through the material. It was discovered in 1857 and occurs in transition ferromagnetic (FM) materials [1]. As we see, the potential of the use of the spin of electrons started to be explored more than a century ago. One of the most important magnetoresistive effects is Giant magnetoresistance (GMR), discovered in 1988

[2]. It is observed in structures composed by two ferromagnetic layers separated by a non-magnetic (NM) spacer, like multilayers or spin-valves (SVs). The phenomenon consists of the change of electrical resistance when the relative angle of the FM layers magnetization (θ) varies. TMR also consists on the change of electrical resistance when θ is varied, but instead of a non-magnetic spacer, the FMs are separated by an insulating material, which leads to a very different physical origin and behaviour of the magnetoresistive effects.

Even though TMR was observed in 1975 by Julliere [3], before the discovery of GMR, it became more relevant with the discovery of TMR at room temperature in amorphous barriers, in 1995 [4], which led to an increase in applications of MTJs in sensors and data storage. With the first reports of high TMR ratios using MgO-based MTJs, this device became one of the most promising technologies for applications in read heads in ultra-high density hard disk drives (> 100 Gb/in^2) and in the promising high density magnetoresistive random access memory (MRAM). Some other applications for MTJs are in novel microwave devices, logic circuits and, most recently, nano-oscillators. Another important discovery in spintronics was the spin transfer torque (STT) effect, which allows to control the magnetic state of a ferromagnetic layer through spin-polarized currents instead of magnetic fields. This offered advantages such as keeping simpler and condensed circuit designs, as well as increasing the scalability of circuits with MTJs, since it became possible to read and write the state of an MTJ by passing current through a single line.

1.2 Magnetic tunnel junctions

Magnetic tunnel junctions are one of the most notable devices that emerged from the Spintronics research field. The simplest MTJ structure comprises two ferromagnetic (FM) layers separated by an insulating layer, which is commonly called the tunnel barrier (TB). In an ideal junction, electrical current can only flow through the insulator through quantum tunnelling, since this is a non-conductive layer with a thickness of around 1 nanometre or less. In this device, one of the ferromagnets has a fixed magnetization direction and the other FM is free to change the direction of its magnetization. These are then called the reference (or fixed) layer (RL), and the free (or sensing) layer (FL), respectively. By the application of an external magnetic field, the free layer can change its magnetization direction, aligning with the direction of the field. This offers two main magnetization states: parallel (P) and antiparallel (AP) alignment, which correspond to different resistance states, R_P and R_{AP}, respectively. This change in resistance of the tunnelling current,

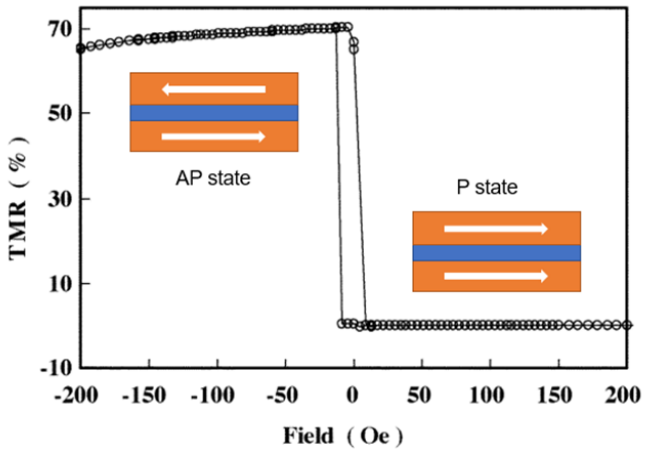

FIGURE 1.1: TMR measured as a function of applied external in-plane magnetic field. The magnetization state is depicted by the main tri-layered structure that composes an MTJ. The AP/P state correspond to the highest/lowest magnetoresistance states. Adapted from [5].

achieved by the application of an external magnetic field, is called tunnel magnetoresistance (TMR). This effect may also be described in terms of electrical conductance (G) in the parallel and antiparallel states, being quantitatively defined as:

$$TMR = \frac{R_{AP} - R_P}{R_P} = \frac{G_P - G_{AP}}{G_{AP}} \ (\%). \tag{1.2}$$

A typical TMR curve, as a function of the externally applied magnetic field, can be observed in Fig. 1.1, as well the correspondent magnetic states.

1.3 Spin polarized tunnelling: Julliere Model

The TMR effect was first described by Julliere [3], in 1975, in a model based on two main hypothesis. The first one is spin conserved tunnelling. This means that electrons can only tunnel from one FM electrode to the other between same spin states. Thus, the tunnelling process is described by a two parallel current path, for spin-up and spin-down electrons. This effect is schematized in Fig 1.2: in the parallel state, majority/minority electrons tunnel to unoccupied majority/minority electron states in the second FM, and in the antiparallel state, majority/minority electrons tunnel to unoccupied minority/majority states in the second FM. The second hypothesis is that the current for electrons in a given spin orientation is proportional to the product between the density of states (DOS) in both FM layers. That said, being N_1 and N_2 the density of states at the Fermi level in the first and

second FM layers, the current density (J) in the parallel and antiparallel configurations can be defined as [3]:

$$J_P \propto N_{1\uparrow}(E_F)N_{2\uparrow}(E_F) + N_{1\downarrow}(E_F)N_{2\downarrow}(E_F), \tag{1.3}$$

and

$$J_{AP} \propto N_{1\uparrow}(E_F)N_{2\downarrow}(E_F) + N_{1\downarrow}(E_F)N_{2\uparrow}(E_F). \tag{1.4}$$

The up arrow $\uparrow$ and down arrow $\downarrow$ represent spin-up and spin-down electrons, respectively, while E_F is the Fermi Energy. This model also relates the DOS with the polarization of the ferromagnets, which corresponds to a measure of the spin-up and spin-down imbalance near the Fermi level, in the following way:

$$P = \frac{N_{\uparrow}(E_F) - N_{\downarrow}(E_F)}{N_{\uparrow}(E_F) + N_{\downarrow}(E_F)}, \tag{1.5}$$

where $N_{\uparrow/\downarrow}(E_F)$ are the density of spin-up ($\uparrow$) and spin-down ($\downarrow$) electron states. The origin of this definition is explained by the electronic bands of the ferromagnetic layers, which have a strong spin imbalance near the Fermi level, since their electron valence band lies in the 3d orbital. This causes an exchange split energy band diagram for spin-up and spin-down electrons, which results in a permanent magnetic moment and spin imbalance near the Fermi level, thus, affecting the conduction of the electrons.

Being P_1 and P_2 the polarization of the first and second ferromagnets, the TMR ratio can be written in terms of polarization:

$$TMR = \frac{2P_1P_2}{1 - P_1P_2}. \tag{1.6}$$

Julliere's model describes TMR in terms of polarization as if this is an intrinsic property of the FM material, with no respect to the tunnel barrier. But in fact, several theoretical works [7–9] showed that the choice of the insulator material, as well as the FM/I interface, play a critical role in the tunnel magnetoresistance. Conductance depends strongly on the symmetry between the Bloch states of the ferromagnets and the evanescent states of the insulator, and even different Bloch states have different decay rates in the tunnel barrier. These considerations are concisely discussed further ahead in Section 2.1 from Chapter 2. Although this model is widely used to describe TMR in magnetic tunnel

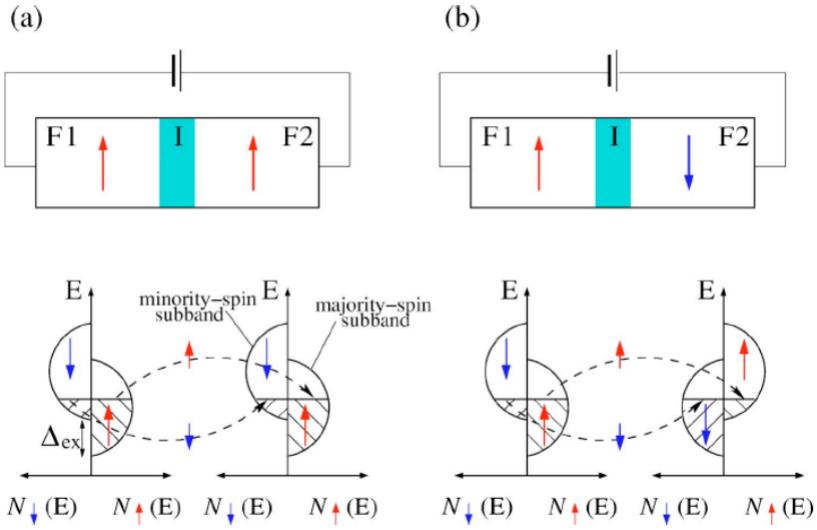

FIGURE 1.2: Schematic illustration of FM/I/FM tunnelling and respective band structure in the (a) Parallel configuration and (b) Anti-parallel configuration of the FMs magnetization. Δ_{ex} represents the exchange slip energy of the sub-bands. Arrows in FM1 and FM2 layers are determined by the majority spin sub-band of each configuration. Taken from [6].

junctions, it disregards other important parameters too, such as impurities in the tunnel barrier, magnon and phonon-assisted tunnelling [10], the detailed-band structure of the materials and the tunnel barrier height.

1.4 Simmon's Model

It is known that the resistive behaviour of an MTJ is non-linear, which is a direct result of quantum tunnelling transport. There are several theoretical models proposed to describe the effect by treating the insulating layer as potential barrier between two similar metallic electrodes. The most recognized is Simmon's model [11], which considers the tunnel barrier to be a rectangular energy barrier, as represented in Fig. 1.3.

This model describes the tunnelling current as depending on free variables determined by each MTJ, namely the barrier thickness and height. In order to determine these parameters, the model for intermediate-voltage range ($eV < \phi_0$) [11] can be used to fit the experimental I-V curves, and is described as:

$$I = A\left\{k_1\left(\phi_0 - \frac{eV}{2}\right)exp\left(k_2\left(\phi_0 - \frac{eV}{2}\right)^{\frac{1}{2}}\right) - k_1\left(\phi_0 + \frac{eV}{2}\right)exp\left(k_2\left(\phi_0 + \frac{eV}{2}\right)^{\frac{1}{2}}\right)\right\}, \tag{1.7}$$

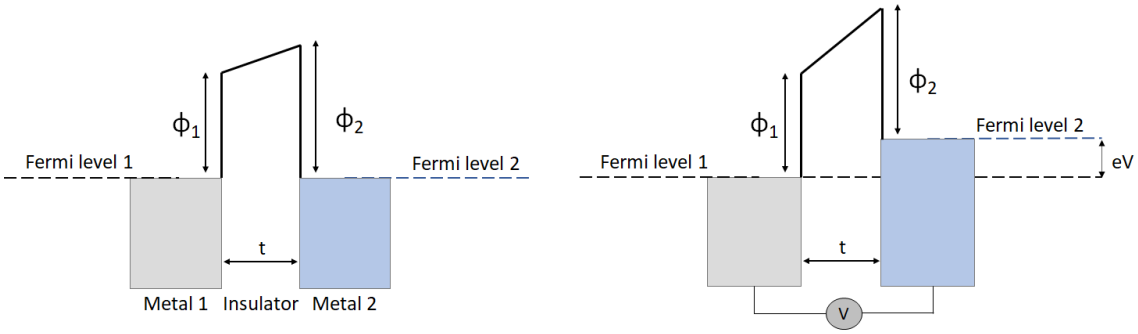

FIGURE 1.3: Schematic representation of the tunnel barrier as a rectangular potential barrier, surrounded by the two FMs, as treated by Simmon's model. t is the tunnel barrier thickness and Φ_1 and Φ_2 are the necessary energies to extract an electron from the Fermi level across the tunnel barrier. In an equilibrium state, the Fermi levels correspond to the same energy. When a voltage is applied across the FMs, an unbalance between the levels is created, generating a tunnelling current.

where t is the thickness of the barrier, ϕ_0 is the barrier energy width, h is Boltzmann's constant, e is the electron charge, m is the electron mass and:

$$k_1 = \left(\frac{e}{2\pi h t^2}\right), \tag{1.8}$$

and

$$k_2 = -\frac{4\pi t}{h}(2m)^{1/2}. \tag{1.9}$$

Although this model fits the experimental curves quite well, one must have in mind that it was developed for AlO_x amorphous barriers, and does not take into account the presence of impurities and pinholes in the barrier [12]. Especially for the samples with Ta particles in the barrier, this particular condition of the junctions is not reflected. One may, though, use the fit to have approximate values and extract the intrinsic characteristics of a pinhole free barrier.

1.5 This thesis

1.5.1 Motivation

In the latest years, new classes of applications for spintronic devices have emerged. The growing need for larger data storage capability and higher data processing speed, comes with the cost of rising energy consumption and environmental damage. With this in mind, spintronics research has grown a branch for spin-assisted energy harvesting, through the

rectifications of thermal fluctuations (as detailed in Section 2.6). The main motivation for this work were the reports on the use of MTJs with embedded paramagnetic (PM) particles for energy harvesting [13], where they take advantage of the fact that oxygen vacancies are one of the most common defects in MgO-based MTJs. To study the effect of doping the tunnel barrier with PM nanoparticles, a monolayer of Ta was deposited in the middle of the MgO barrier, forming a CoFeB/MgO/Ta(0.06nm)/MgO/CoFeB barrier. Using tantalum, we aim to take advantage of the fact that this is one of the materials used in commercial MTJs, so that it would be very easy to integrate it in the structures. Plus, there is a large number of studies concerning the presence of impurities in amorphous AlO_x barriers, but not so much in MgO crystalline insulating layers. Besides this main purpose, there are many intrinsic properties of the device which are extremely influenced by the existence of any kind of particles, defects or impurities in the MTJ structure. The first MTJs presented a TMR value of only a few percent. Nowadays, TMR ratios go over 600% at room temperature. This achievement was possible not only due to a better understanding of these physical properties, but also due to the development of fabrication techniques, that allowed to produce almost perfect devices. In this case, the presence of PM particles in the tunnel barrier will affect several aspects of the physical properties, which are extremely appealing to study for itself. How impurities affect the electronic structure of MTJs is of high technological interest [14], since the requirements for applications are getting more demanding.

Thus, this work aimed not only to study the energy harvesting feature, but also how defects shape the physical properties of magnetic tunnel junctions.

1.5.2 Thesis organization

After the overview on the main aspects underlying an MTJ presented in this chapter, the next chapters are organized in the following way: Chapter 2 contains the different types of tunnelling in an MTJ, as well as its the basic structure. It also contains a section exploring the Energy Harvesting effect we aim to study in this thesis. Chapter 3 consists on the experimental techniques used in this thesis. It comprises a description of the fabrication techniques performed at INL to fabricate the MTJs, and the characterization techniques used to study the devices. Chapter 4 contains the obtained experimental results, in hand with the analysis of the origin behind the observed behaviours. Finally, in Chapter 5 the

main results and final conclusions are presented, as well as some considerations on future work.

Chapter 2

Magnetic Tunnel Junctions

2.1 Tunnelling through a crystalline barrier

2.1.1 Bloch states and symmetry groups

The critical effects in magnetic tunnel junctions occur at the interfaces between the ferromagnetic layer and the tunnel barrier. Only electrons with Bloch states that couple with evanescent states from the tunnel barrier can be transmitted from one electrode to the other through quantum tunnelling, which critically affects the TMR ratio. Evanescent Bloch states are not allowed in infinite systems, since they diverge, but in finite systems they can be normalized, and have decay rates which depend on spacial symmetries.

An electron propagating through a single crystal system is subjected to a potential with the same periodicity as the crystal, and its state is described by Bloch wave functions $\phi(r)$, which can be written as [15]:

$$\Phi_k(r) = u_k(r)exp(ik \cdot r), \tag{2.1}$$

where u_k is a function with the periodicity of the lattice and k is the particle's wave vector.

Bloch states can be grouped in regard to spacial symmetries, due to the electronic state of electrons, and so, due to their atomic orbitals. Figure 2.1 represents different atomic orbitals and respective symmetry groups that couple with the MgO barrier. These symmetries have a crucial role in the tunnelling of electrons, by determining the number of nodes of the wave function in the plane parallel to the interface, that increase the decay rate perpendicular to the propagation direction, and describe correctly the attenuation rates in MgO barriers [16].

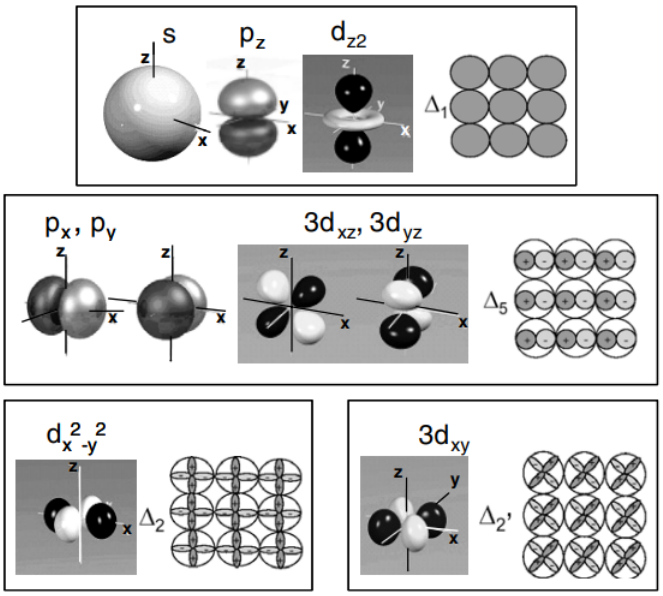

FIGURE 2.1: Representation of atomic orbitals grouped by symmetry: Δ_1 (s, p_z,$d_{z^2-r^2}$ orbitals), Δ_5 (p_x, p_y, $3d_{xy}$ and $3d_{yz}$), Δ_2 ($d_{x^2-y^2}$) and $\Delta_{2'}$ ($3d_{xy}$). Taken from [16].

MgO is a non-magnetic electric insulator, with a large band-gap. Its crystalline structure is composed of Mg^{+2} and O^{-2} ions. It forms a rock-salt face-centred cubic (fcc) structure along the (001) direction.

2.1.2 MgO spin-filtering mechanism

Butler [17] calculated the transmission probability for Bloch states, propagating in a Fe/MgO/Fe structure, that can couple with evanescent sates of the MgO barrier. Calculations were performed considering only states with a null parallel wave vector component, $k_{\|} = 0$, where $k_{\|}$ is the component of the wave vector parallel to the plane of the Fe/MgO interface. Each symmetry group presents different transmission probability, which depend on the interfacial transmission probability and on the decay rate of each group of functions [17].

For the parallel state, in the majority-majority $\uparrow\uparrow$ channel (Fig. 2.2(a)), there are Δ_1, Δ_5 and $\Delta_{2'}$ states propagating, from the first electrode, but Δ_5 and $\Delta_{2'}$ have very large decay rates comparing to Δ_1, which has the largest transmission probability. In the minority-minority $\downarrow\downarrow$ channel (Fig. 2.2(b)), Δ_5, $\Delta_{2'}$ and Δ_2 keep a similar behaviour, but there are no Δ_1 electrons. This leads to a conduction in the parallel state dominated by the majority-majority channel. For the case of anti-parallel alignment, for both majority-minority ($\uparrow\downarrow$)

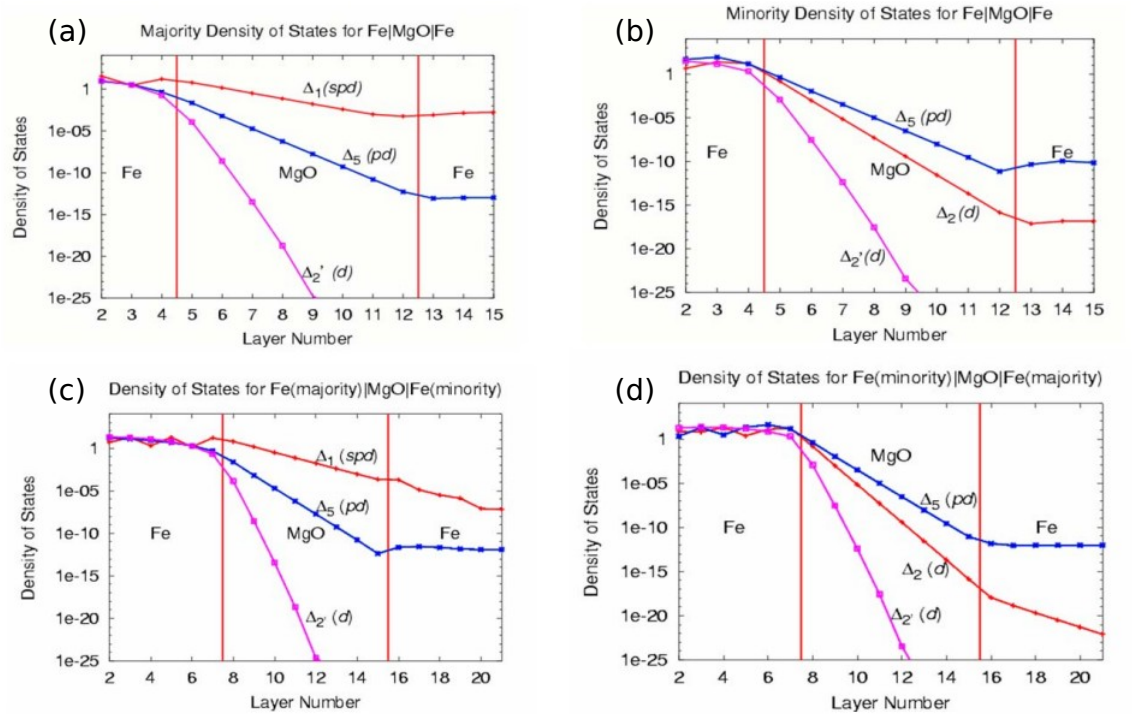

FIGURE 2.2: Tunnelling DOS calculation for electrons tunnelling in a Fe/MgO/Fe structure. Graphs show the contribution from each symmetry group to (a) $G^{\uparrow\uparrow}$, (b) $G^{\downarrow\downarrow}$, (c) $G^{\uparrow\downarrow}$ and (d) $G^{\downarrow\uparrow}$. Adapted from [17].

and minority-majority ($\downarrow\uparrow$) channels, Δ_5, $\Delta_{2'}$ and Δ_2 have a very large decay rates. Concerning Δ_1 electrons, in the majority-minority channel they are transmitted, but the wave function is still decaying in the second Fe electrode, so they will have a minor contribution to the conductance. In the minority-majority channel there is no contribution to the conductance from these electrons. This said, one concludes that conductance in the P state is much larger than in the AP state. This means that combining the MgO tunnel barrier with FM materials which have propagating Δ_1 Bloch sates at the Fermi level, in one of the spin channels but not the other, turns MgO into a spin filter.

2.1.3 Incoherent tunnelling through an amorphous barrier

The first MTJ devices commonly contained an amorphous aluminium oxide (AlO_x) tunnel barrier, since this material provided greatly coherent layers [17]. But amorphous layers do not present any crystallographic symmetry. Thereby, Bloch states with various spacial symmetries can couple with the evanescent states from the barrier. Unlike in crystalline barriers, there is a non-zero tunnelling probability for all Bloch states. This is called incoherent tunnelling. The maximum TMR ratio obtained at room temperature using AlO_x

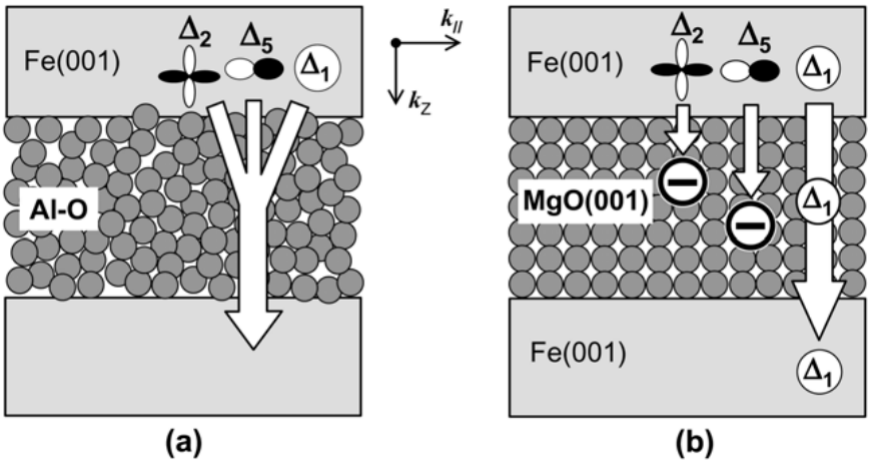

FIGURE 2.3: Schematic illustration of (a) incoherent tunnelling through an amorphous barrier and (b) coherent tunnelling through a crystalline barrier. Taken from [20].

is of 81% [18], a value that cannot compete with the maximum of 604% [19] obtained at 300 K using an MgO barrier, which presents the previous discussed coherent tunnelling mechanism. In Fig. 2.3 the tunnelling mechanisms of both an amorphous and crystalline barrier are illustrated, for the case of Fe(001) electrodes.

Julliere's model admits the same tunnelling probability for all symmetry groups, which is a consequence of an incorrect definition of the polarization. As an example, considering the band structure of Ni and Co to calculate the polarization using Eq. 1.5, results in a negative P value, but experimental results [21] show that P is positive when these materials are combined with the AlOx barrier. This indicates that the tunnelling probability depends on the symmetry of the Bloch state. Therefore, it is considered that the tunnelling process in an amorphous barrier is a mixture of incoherent and coherent tunnelling.

2.2 MTJs structure

As mentioned, the main components of an MTJ device comprise a FM/I/FM tri-layered structure. However, an MTJ is a multilayered nanostructure that comprises several other layers, each with a designated function, turning the MTJ into a complex device. A typical MTJ structure is presented in Fig.2.4:

From bottom to top, this junction contains: a buffer layer (BL), which favours a particular growth direction for the other layers; an antiferromagnetic pinning layer (AFL); a synthetic anti-ferromagnetic structure (SAF), which is a three layers FM1/NM/FM2 structure (ferromagnet/non-magnetic/ferromagnet), being the FM2 the reference FM layer;

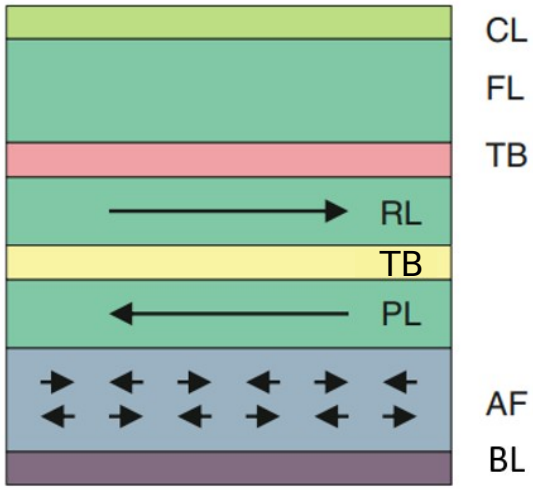

FIGURE 2.4: Magnetic tunnel junction structure. Adapted from [22].

an electric insulator (I), which corresponds to the tunnel barrier (TB); a sensing layer (FL); and finally, on top, a cap layer (CL), responsible for protecting the structure from mechanical and chemical damage. The free layer is able rotate the direction of its magnetization, in response to applied external magnetic fields, but the magnetization of the lower ferromagnet is fixed. This is achieved through the incorporation of the fixed FM in a SAF structure, deposited on top of antiferromagnetic (AFM) layer. The AFM creates a unidirectional magnetic anisotropy in the lower layer of the SAF structure (FM1), by exchange bias. The SAF structure is antiferromagnetically coupled by the RKKY (Ruderman–Kittel–Kasuya–Yosida) interaction, which guarantees the pinning of the FM2. This mechanism is mediated by the spacer (non-magnetic layer) thickness. It produces a more stable reference layer, since it provides stronger exchange bias and a smaller stray field acting of the free layer [20], which are advantages over a simple AFM layer.

2.3 Voltage dependent transport

Conductance and tunnelling magnetoresistance present significant dependence with an applied external bias voltage (V) across the tunnel junction. In most junctions, the TMR ratio decreases significantly with bias and the behaviour should be symmetric around zero applied bias, for electrodes of the same FM materials. A convenient parameter in the characterization of an MTJ performance is its figure of merit $V_{1/2}$ [23], which corresponds to the voltage at which the value of TMR reaches half of its maximum value, $TMR(V_{1/2}) = TMR(0)/2$. It characterizes the quality of the interface between the FM

and the tunnel barrier, and is quite important in sensor applications, since it indicates how the TMR behaves with bias. Several mechanisms contribute to the dependence on bias, such as inelastic scattering through magnon excitations, photon assisted tunnelling, impurity assisted tunnelling and of course, the electronic band structure of the FM electrodes.

Magnon and phonon assisted tunnelling. The first mechanism, suggested by Zhang. el al. [24], considers that the excitation of magnons at the FM/insulator interfaces causes inelastic electron scattering. When a non-zero bias voltage is applied, conducting electrons that have tunnelled from one electrode into the other, with higher energy than the Fermi energy of the electrode (hot electrons), might lose this additional energy through the emission of a magnon, that is, exciting local spins and flipping its own spin; therefore, there is no spin conservation in this process. With increasing voltage, more magnons are emitted, causing a reduction on the TMR and the resistance of the MTJ. Phonons may also contribute for the dependency of conductance on voltage [10], when the tunnelling of an electron is accompanied by the emission or absorption of a phonon. The contribution from phonons to the conductance is opposite from the one by magnons, since this is a spin-conserving mechanism, reducing the negative effect of magnons.

Band structure. The band structure of electrodes also plays an important role in the voltage dependence of the conductance [25]. With increasing bias, electrons tunnel from occupied energy states below the Fermi energy states of one electrode, to unoccupied states above the Fermi level of the second electrode. This diminishes the difference between majority and minority electronic states, which lowers the polarization and, consequently, the TMR ratio. This effect depends on the electric configuration of the electrodes, and on their band structure.

Impurity assisted tunnelling. A model presented by Zhang and White [26] suggested that one of the most significant aspects in the V-dependency of TMR is the presence of impurities in the tunnel barrier. Impurities might generate different mechanisms, creating additional conductance paths for electrons, that cause a decrease in the TMR. Assisted tunnelling through induced defects in barrier is a mainly elastic process.

2.3.1 Inelastic Electron Tunnelling Spectroscopy

Inelastic Electron Tunnelling Spectroscopy (IETS) is a characterization technique developed to study the underlying inelastic tunnelling mechanisms in MTJS. This technique

consists in measuring the bias dependence of the total current crossing the insulating barrier of the MTJs, from which one can obtain d^2I/d^2V (dG/dV) [27], that corresponds to the IETS spectra. Inelastic mechanisms, such as magnons and phonons, are identified as peaks in this spectra. If the applied bias is such that it causes a separation of the Fermi level equal to the inelastic energy loss of an inelastic interaction, a conduction channel is created and a slope in the current will appear [28], creating a peak in the second derivative. So, these peaks correspond to additional conduction channels for tunnelling electrons [29], besides direct tunnelling. Another feature commonly present in MTJs conductance curves, which can be identified in the IETS spectra, is the zero-bias anomaly (ZBA), characterized by a conductance peak around zero bias voltage. This is translated into a large peak in the IETS spectra. This anomaly might originate from inelastic mechanisms, such as magnons, which contribute to the deviating conductance behaviour. Plus, spin-flip processes of inelastic nature can take place in the presence of paramagnetic impurities (impurity assisted tunnelling) [30], creating this anomaly.

Besides inelastic processes, this technique is also viable for elastic processes [27], such as trap assisted tunnelling, which originates from the presence of traps in the TB. Traps can affect conduction in opposite ways, depending on their nature, creating two different processes: (1) trap-assisted conduction and (2) trapping of carriers. In the first process, conductance is favoured, creating an increase in the electrical current. In the IETS spectra this corresponds to peak follow by a valley. In the second process, charge trapping occurs, causing a decrease in conductance. This originates a valley followed by a peak in the spectra. These elastic processes are distinguishable from other inelastic processes, since these are the only features that are represented by both peaks and valleys, unlike vibrational modes, e.g., magnons and phonons, which are represented solely by either peaks or valleys. The shape of the features should be similar for positive and negative bias. If a feature appears twice, for the same external bias, but with opposite signs, it means that they are originated from the same trap, but in different tunnelling directions. The difference in intensity between peaks may be due to asymmetries in the tunnel barrier [23].

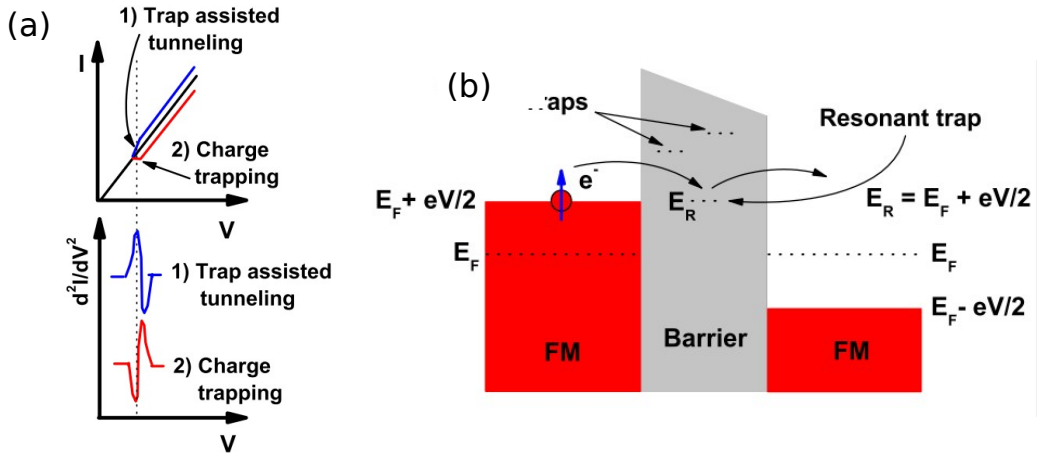

FIGURE 2.5: (a) Scheme of two types of traps unveiled by the IETS technique. (b) Representation of the tunnel barrier and FMs, with an applied bias such that the energy of the trap corresponds to Fermi level of the left FM, allowing a process a trap assisted process. Adapted from [23].

2.4 Temperature dependent transport

Temperature is a strong factor in the variation of tunnel magnetoresistance in a tunnel junction. Namely, as the temperature increases, a clear decrease in the TMR ratio is usually observed. Several effects can be responsible for this behaviour, such as thermally exited magnons in the electrodes, variation of the electronic structure of the device and the excitation of defects or impurities in the electrode/tunnel barrier interface. As can be seen in Fig. 2.6, the resistance in the anti-parallel state has a much stronger dependency than in the parallel state. This said, the TMR enhancement at low temperatures is usually mainly due to the variation in R_{AP}. Several tunnelling phenomena can contribute to the conductance too, such as direct tunnelling, hopping via localized states in the barrier, scattering at magnetic impurities and magnon/phonon assisted tunnelling [31].

Shang presented a model to describe the temperature dependence of the conductance in an MTJ [33], which is based on Julliere's work [3], but modified by considering the contribution of two different conduction channels: spin-dependent direct elastic tunnelling, and assisted spin-independent tunnelling. The total conductance is then described in the following way:

$$G(\theta) = G_T[1 + P_1 P_2 cos(\theta)] + G_{SI}. \tag{2.2}$$

In this expression, G_T is a prefactor for direct elastic tunnelling, P_1 and P_2 are the spin polarization of the ferromagnets and θ is the angle between the magnetization of the

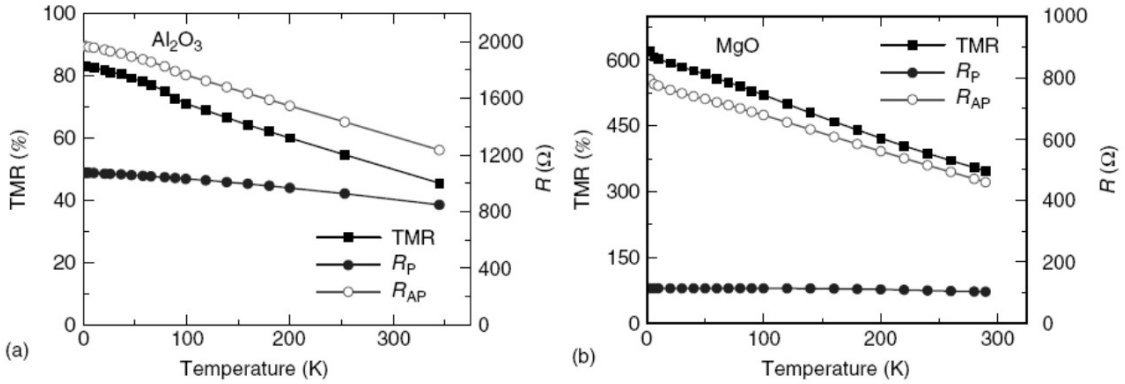

FIGURE 2.6: Example of TMR, R_P and R_{AP} temperature dependence of a (a) Al_2O_3 and (b) MgO based MTJ. Adapted form [32].

FM electrodes ($\theta = 0°$ and $\theta = 180°$ for the P and AP state, respectively). The second conductance term, G_{SI}, is a term for non-polarized conductance, therefore, independent of the magnetization of the electrodes. According to theory, derived by Simmons [34], the prefactor G_T can be written as:

$$G_T = G_0 \frac{CT}{sin(CT)}, \tag{2.3}$$

where G_0 is a constant that corresponds to the conductance at null temperature, and $C = 1.387 \times 10^{-4} d/\sqrt{(\phi)}$, being d the barrier width ($\AA$) and ϕ the barrier height (eV). The G_T dependence on the temperature arises from the broadening of the Fermi distributions of the electrodes, although such variation is subtle [33]. The additional spin-independent term in conductance, G_{SI}, is introduced considering hopping of electrons through localized states in the tunnel barrier, which can have origin in either defects or non-magnetic impurities. Since it in a non-polarized term, it will contribute negatively to the TMR, by increasing the conductance as temperature increases [33]:

$$G_{SI}(T) = \sum n S_n T^{n-\frac{2}{n+1}}, \tag{2.4}$$

where n corresponds to the number of hopping sites and S_n is a prefactor related to the density of hopping states. This model also introduces the variation of the electrodes polarization with temperature, which is considered to vary with T in the same way that the magnetization (M) does, in accordance to Bloch-law:

$$M(T) = M_0(1 - \alpha T^{3/2}) \tag{2.5}$$

where M_0 is the magnetization at 0 K and α is a material dependent constant. The $M(T)$ dependence is explained in terms of thermal spin excitations in the FM electrodes. Thus, the T-dependence of the polarization is described as:

$$P(T) = P_0(1 - \alpha T^{3/2}). \tag{2.6}$$

Here, P_0 corresponds to the polarization at 0 K. Both P_0 and α are very much affected by interfacial contamination [35]. According to the considerations described in this model, the TMR equation described by Julliere is now modified by the introduction of the terms for direct elastic tunnelling and unpolarized conductance, being written as:

$$TMR = \frac{2P_1P_2}{1 + P_1P_2 + \frac{G_{SI}}{G_T}}. \tag{2.7}$$

Other mechanisms that affect the variation of TMR with temperature are phonon and magnon assisted tunnelling. In the first case, temperature causes the excitation/absorption of phonons at the FM electrodes [10]. In the case of magnons, Zhang [24] proposed that inelastic scattering due to magnon excitation at the FM/TB interface decreased the TMR ratio, resulting from spin-flip processes. In the P state, a spin-flip process occurs, where majority tunnelling electrons are scattered to minority states, and vice versa. As for the AP alignment, tunnelling majority/minority electrons are scattered to majority/minority states. Similarly with the bias influence, with increasing temperature more magnons are created, and the TMR decreases. Another contribution could be from the excitation/absorption of phonons, which corresponds to an inelastic spin-conserving mechanism.

2.5 Different tunnelling mechanisms

In the latest sections, the different aspects to be considered in terms of how temperature and voltage variation affect tunnelling have been discussed. Our system consists of a magnetic tunnel junction with embedded paramagnetic tantalum nanoparticles in the tunnel barrier. Besides direct elastic tunnelling, that was accounted in Julliere's theory, there are other different tunnelling mechanisms, which are difficult to analyse independently. In the present section, some of the possible tunnelling regimes are further discussed.

Resonant Tunnelling The presence of impurities in the tunnel barrier can lead to resonant tunnelling, if the electronic levels of the impurities are close to the energy of the system (lie close to the chemical potential of the system) [30]. Theory predicts that resonant tunnelling through magnetic impurities enhances TMR [36], in contrast to non-magnetic (NM) impurities, which decrease the TMR. Impurity-assisted resonant tunnelling is only expected for impurities in the centre of the barrier and near the Fermi level. Plus, the defects are expect to contribute to the TMR in smaller area junctions.

Inelastic Co-Tunnelling Inelastic co-tunnelling is a mechanism that dominates at low temperatures, namely in the Coulomb Blockade regime. This process consists of the tunnelling of an electron from the left lead into a virtual state of a nanoparticle, and also the tunnelling of another electron from the dot to the right lead, creating a two step process where the charge of the nanoparticle in unchanged.

Coulomb Blockade Coulomb Blockade is a regime in which electron tunnelling into a small particle is significantly suppressed, at low temperatures, decreasing the electrical conductance. This is due to increasing charging energy of the particles when their capacitance is very small [37]. When the tunnelling of one electron into a small particle occurs, the particle is charged by an elementary charge. The energy of the system is enhanced by $E_C = e^2/2C$, where e is the electron charge and C is the capacitance of the particle. Small particles usually have small capacitance, which means that the charging energy will strongly exceed thermal energy (k_BT).

This effect can be observed in different systems, such as semiconductor heterostructures. When CB suppresses direct tunnelling, TMR is expected to be enhanced, since only co-tunnelling processes are allowed [38]. This effect is only relevant at low temperatures, when charging energy E_C is much larger than thermal energy E_T. This effect is also expected to be absent if electrodes are not spin polarized.

2.6 Energy harvesting

Spintronics finds its most common application field in data storage and sensors. However, a new class of spintronic devices has emerged in the latest years, as its unique properties allow to explore new functionalities and flexibility in electronic devices. Energy harvesting has always been a relevant topic, and as the necessity for novel ways of generating more energy and in a more sustainable way grows, different branches of science have opened routes toward this goal.

Concerning spintronics, nano thermoelectric devices are a common research topic towards power generation. The key idea behind this technology is the rectification of thermal fluctuations in mesoscopic conductors. There are prosper reports on conjugating quantum dots with thermoelectric devices, which could operate with higher efficiency than usual thermoelectric devices. These devices lay in the category of quantum spin heat engines, since they rely on a temperature gradient ΔT to produce electrical energy. However, there are very recent reports on purely spintronic engines [13, 39, 40], producing power at thermal equilibrium. The first experiments on this type of engine reported the use of spin-split paramagnetic centres to harvest thermal fluctuations [39, 40]. There is also a recent report on using MgO-based magnetic tunnel junctions with paramagnetic centres in the tunnel barrier to generate power, with a maximum achieved output of around 0.1 nW. The maximum power output is of 42 nW at room temperature, recorded in [41]. The sections ahead will present a small discussion on the working principles of the device. In this thesis, we aim to reach the same effect using tantalum paramagnetic centres in the MgO tunnel barrier. These kind of engines could be used in spin batteries [39], energy harvesters [40] and low-power magnetic sensors or information storage [13].

2.6.1 Spintronic selector and paramagnetic centre

The report in Ref.[13] experimentally demonstrated that a magnetic tunnel junctions containing paramagnetic centres with spin-split energy in the tunnel barrier can produce a spontaneous spin-polarized electrical current, generating power. The critical elements necessary to observe the effect in the tunnel junction are paramagnetic centres with spin-split energy between states, lower than the thermal energy $k_B T$, and the presence of spintronic selectors. To explain the effect in more detail, let us consider the MTJ setup schematized in Fig. 2.7.

The figure depicts the FM electrodes as spintronic selectors. A spintronic selector is a material which preferentially favours one spin-channel transport, blocking the other [13]. Its purpose is to control the symmetry/asymmetry of the energy profile in the system. In a tunnel junction, this is accomplished by the FM/MgO interface [13]. As discussed in the previous chapter, in the anti-parallel state, the ferromagnets offer a very strong spin-dependent transmission rate. For a symmetric energy profile, the spontaneous tunnelling rates for charge carriers from each lead are equal. Introducing an asymmetry will generate different tunnelling rates, therefore, creating a spin-unbalance. This means that a

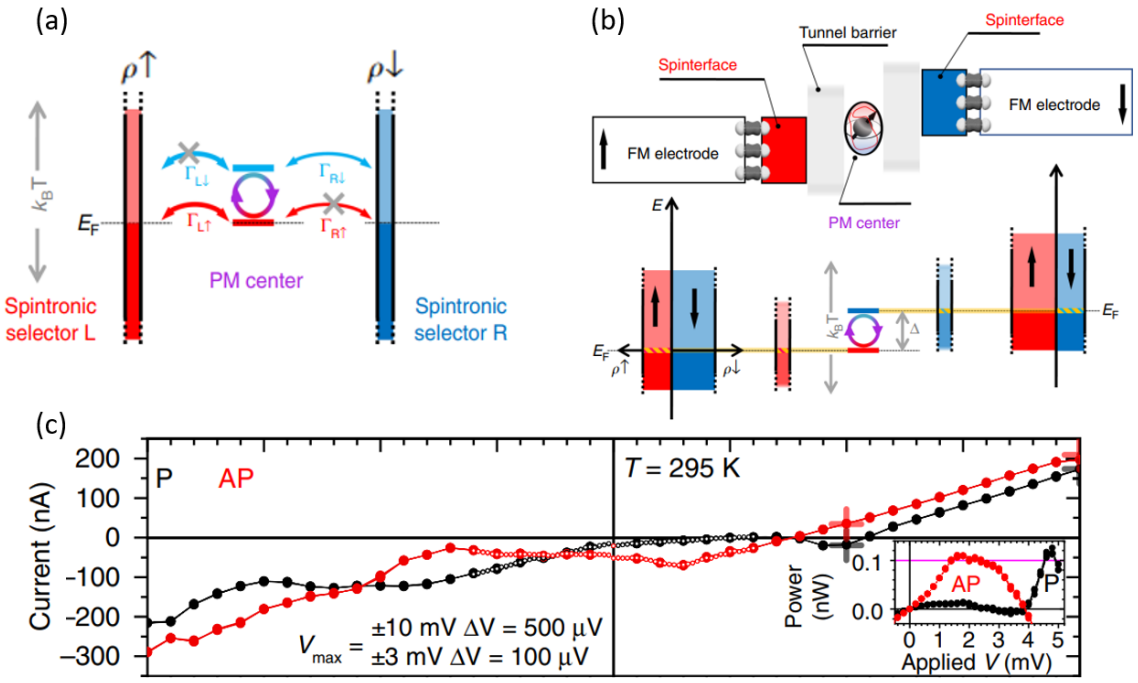

FIGURE 2.7: (a) Schematic of the spintronic selectors with a single PM centre in the middle, and the spin tunnelling rate asymmetry between leads. $\tau_{L\uparrow/\downarrow}$ and $\tau_{R\uparrow/\downarrow}$ correspond to the tunnelling rates of electrons with $\uparrow/\downarrow$ spin states, between left lead and PM centre, and right lead and PM centre, respectively. (b) Energy landscape in across the MTJ containing a PM centre, in the AP state. The Fermi energy (E_F) of the FMs is shifted by an energy Δ, corresponding to the spin-split energy in the PM. Blue/red correspond to $\downarrow$ / $\uparrow$ spin states. (c) Current-voltage curves obtained for both AP and P states, at room temperature. Adapted from [13].

spontaneous current is flowing across the device. This constitutes the basic operation of the spin-engine integrated in a tunnel junction proposed in the work. Due to the combination of the selectors and PM centres, electrons can only tunnel from the PM centre to an electrode if their energy is the same as the PM's centre spin state [13]. In that work, the spintronic selectors consist of a C/MgO interface, and the paramagnetic centres consist on carbon atoms present in oxygen vacancies on the MgO barrier.

The generated spontaneous current across the MTJ is represented by an offset in the current-voltage curves (Fig. 2.7 (c)) . In this thesis, the same setup is used, but the paramagnetic centres consist in Ta particles deposited by magnetron sputtering in the middle of the tunnel barrier, as will be clarified in the experimental techniques chapter (Chapter 3).

Chapter 3

Experimental Techniques

In this chapter, a condensed explanation of the techniques used to fabricate and characterize the studied devices is presented. The first section presents the deposition and micro-fabrication techniques used to fabricate the devices. In the second section, the characterization techniques and set-up are described. All the samples were fabricated at INL and their characterization was performed at IFIMUP.

3.1 Fabrication techniques

The first step in the fabrication of the MTJ devices is the deposition of the different layers of materials that compose the stack. This is performed through a physical vapour deposition (PVD) technique, namely, magnetron sputtering. Several lithography processes are necessary to define the MTJ pillars and electrical contacts on the sample. Direct laser writing (DWL) is used to expose the mask used in the lithography and define the MTJ pillar. The etching processes are performed using a Nordiko 7500 Ion Milling etching system. All these proceedings are performed in a cleanroom environment.

After fabrication, MTJs are subject to a 3-step annealing process, to crystallize the different layers and create an easy magnetization axis on the ferromagnetic layers. In order to crystallize the CoFeB/MgO/CoFeB structure, a first annealing step is necessary, in which a 2 T field is applied for 2 hours, at 330°C. This first annealing induces a uniaxial anisotropy in the magnetic layers and MgO barrier. The second annealing is necessary to rotate both top and bottom AFM, but without rotating the SL. So, a 2 T field is applied for 2 hours at 270°C. Finally, the third annealing step rotates the top AFM layer, which is part of the sensing structure, using a 0.02 T field, at 150°C for 1h. Annealing is an absolute

necessary step for the performance of the device, since it is responsible for creating the crystallographic direction of both FMs and MgO, which leads to higher TMR ratios.

3.1.1 Magnetron Sputtering

Sputtering is a PVD technique used to deposit a certain material in a substrate, through ion bombardment. A sputtering system consists of a vacuum chamber, which contains one or several targets composed of the material one wants to deposit, and a substrate. A inert gas, usually argon (Ar), is introduced in the vacuum chamber and a bias voltage is applied across it, between the target and substrate. Free electrons flow from the negatively charged target (cathode), colliding with the atoms that compose the gas, which results in the ionization of the gas, forming a plasma. The bias signal can be direct current (DC), for the deposition of metals, or a radio frequency (RF) signal, for oxides and insulating materials (to prevent the build-up of charges in the target). Cations formed in the plasma are attracted towards the target at high velocity, ejecting target atoms that will cross the chamber and condensate on the substrate, forming thin films. The magnetron sputtering system contains magnets that create a magnetic field parallel to the target, in order to trap the plasma near it, through Lorentz force, as can be seen in Fig. 3.1(c). The magnetron sputtering technique leads to better quality films than other sputtering techniques, since the trapping of the plasma creates a higher chance of gas ionization near the target, increasing the plasma density in this region. So, creating a magnetic field, the bombardment of the target is increased and so is the deposition rate [42].

The sputtering system present at the INL clean room is composed by a cassette, a transport, soft-etch/oxidation and multi-target modules. The cassette is where the wafers are introduced and the transport module is responsible for mechanically transporting the wafer between the different modules. In the soft-etch module, an RF signal is applied to do a pre-cleaning of the wafer before depositing the materials. This is necessary since, in spite of being inserted in a cleanroom environment, there is the possibility of unwanted particle deposition on the wafer, such as water molecules, or the formation of oxides. The multi-target module is integrated in the ultra high vacuum (UHV) deposition chamber. There are 11 targets available, so it is possible to deposit all the different materials without breaking vacuum. The substrate is moved linearly back and forward across the chamber, so a dynamical deposition occurs. That said, in order to control the deposition rate and

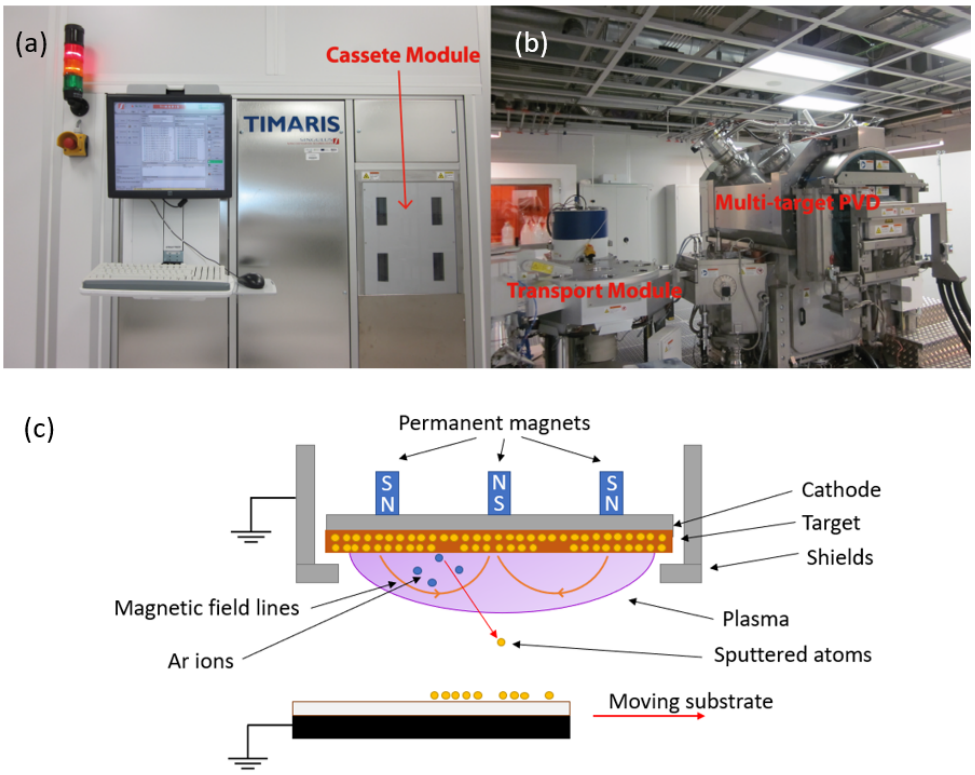

FIGURE 3.1: Magnetron sputtering machine present at INL, used to fabricate the devices in this thesis: (a) cassette module, (b) transport and multi-target chamber. Taken from [43]. (c) Simple schematic of a magnetron sputtering system.

the film thickness, the important parameters are the linear velocity of the substrate and the number of cycles (back and forward) the wafer performs, respectively.

To be able to deposit a 0.06 nm layer of Ta particles in the middle of the tunnel barrier, the deposition conditions had to be adjusted: the velocity of the substrate was at maximum speed, and the plasma frequency was adjusted, so that the plasma had the minimum power possible, while remaining stable. This way, the smallest quantity of material is deposited. Since there is such small quantity of material, the particles are not expected to form isles nor clusters, but remain uniformly distributed across the layer, like small impurities in the barrier.

3.1.2 Ion Milling - Dry Etching

Ion beam milling is a dry etching technique, used to remove atoms from the surface of the samples. An ion beam, which can be made of argon cations, is accelerated in a certain direction, to hit the surface in a specific angle and remove material. This is then a purely

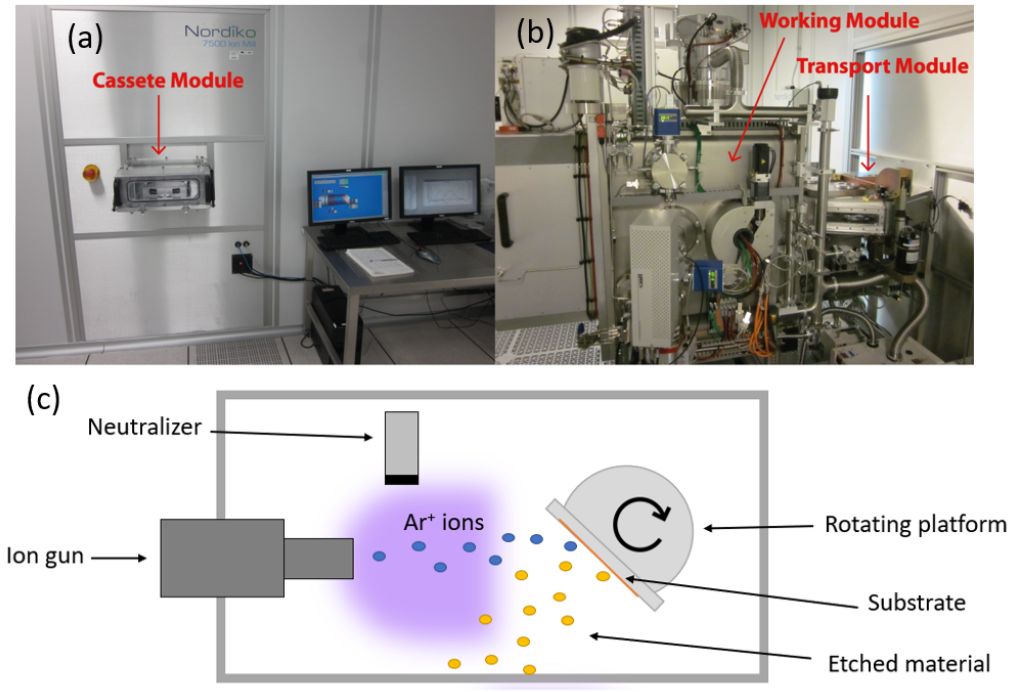

FIGURE 3.2: Nordiko 7500 - physical etching tool used to fabricate the junctions studied in this thesis (at INL): (a) cassette module, (b) transport and working module. Taken from [43]. (c) Simple schematic of an ion mill etching system.

physical process. The ion mill machine used in the INL clean room is a Nordiko 7500, composed of a cassette, a transfer module, and a module consisting of the ion beam source and the vacuum chamber. The ion beam source generates and accelerates the beam towards the sample: An inert gas (Argon) is inserted in the discharge chamber, and plasma is generated by the application of an RF field, generated by an RF source. The argon cations that are formed in the plasma are accelerated towards the sample, and atoms are ejected. There are also electron sources in the chamber, denominated neutralisers, responsible for keeping the total charge neutral. Emitted electrons react with cations, creating a neutral particle, and this way preventing build-up of charges on the sample surface during the etching process. Samples are also subjected to side wall cleaning (SWC), which is an ion milling process performed at a lower angle and shorter intervals, necessary due to the re-deposition of atoms in the surface while the wafer is in the chamber.

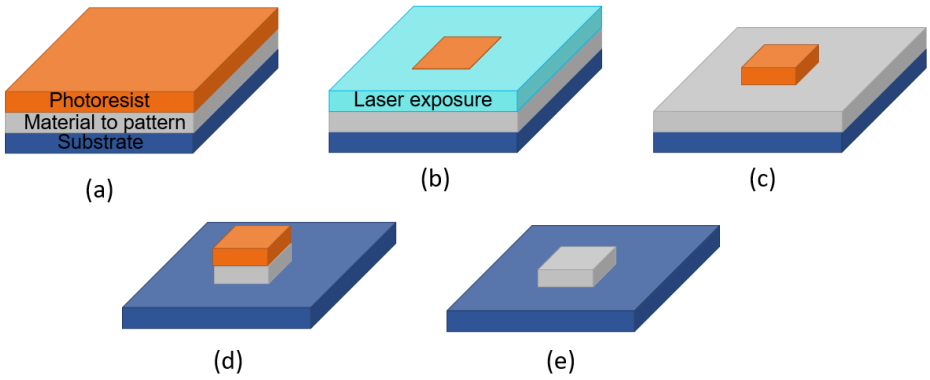

FIGURE 3.3: Lithography steps to define the MTJs pillars. (a) After vapour priming, the substrate is coated with photoresist. (b) The material is laser exposed, in accordance to the digital mask. (c) The exposed PR (positive) is removed in a developing step. (d) The material under which the PR was removed, is also removed in the ion milling. (e) The remaining PR is removed using plasma etching, leaving the desired patterned material.

3.1.3 Direct Laser Writing - Maskless lithography

Several lithography processes are necessary to define the different components of the device. The structures are defined using the Direct Laser Writing (DLW) technique, but the lithography starts with vapour priming, to prepare the surface for the photoresist coating. Then, the wafer is coated with the photoresist (PR), which is a photo-sensitive material that will respond to the writing. After the PR coating, the wafer can be aligned in the DWL table. Then, a laser will expose the PR according to the desired pattern, which is defined as a digital mask designed in the AutoCAD software. At INL, the machine available is a DWL 2000 tool, by Heidelberg instruments. It uses a diode laser of 405 nm, with a minimum feature of 1 μm. After exposure, the wafer is developed, a process in which PR is removed, leaving the desired pattern in the wafer. The remaining PR is removed through plasma etching. In this thesis, a positive PR was used, which means that the PR exposed to the laser is made soluble to the developer, being removed in this step.

3.2 Characterization techniques

The characterization methods used to study the MTJs samples are presented in this section, namely the room temperature setup and the cryogenic system used to study the behaviour of the MTJs at different temperatures. All the data was obtained at the IFIMUP labs at FCUP.

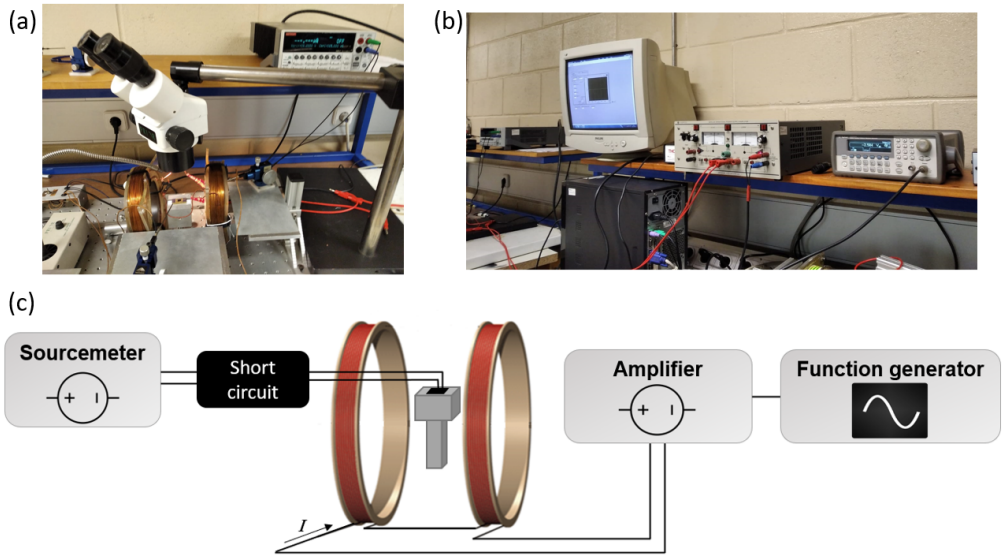

FIGURE 3.4: Room temperature measurement setup: (a) Helmholtz coils, probes, sample holder, and sourcemeter; (b) Computer with LabView software, amplifier and function generator (from left to right). (c) Scheme of the main components of the setup.

3.2.1 Room temperature characterization

The setup used to do a first RT characterization is composed as follows (Fig. 3.4). Helmholtz coils are used to generate a linear magnetic field. The field is controlled by a signal generator, which is used to send an electrical current, and is connected to an amplifier to enhance this current. The actual field is measured using a gaussmeter. A sourcemeter is used to both apply current to the samples, and read the generated voltage. This is performed using two probes, connected to the sourcemeter, that lay on the MTJ pads. The instruments are connected to a LabView software, through a GPIB interface, allowing to control all the applied variables on the sample, and also visualize the results.

3.2.2 Cryogenic measurements

The study of temperature dependent properties of the MTJs was performed using a cryogenic system with a closed helium circuit, where a minimum temperature of approximately 28 K can be achieved.

Sample-holder and chip carrier. The studied MTJs were placed on a chip carrier, since it was not possible to establish electrical contacts directly with the MTJs pad inside the cryostat, due to their micrometric size. So, these pads were wire bounded to the gold pads of the chip carrier. The sample holder, where the chip carrier is placed, consists of a cylindrical block of copper, fixed to the cryostat arm. It contains a cavity with lateral size

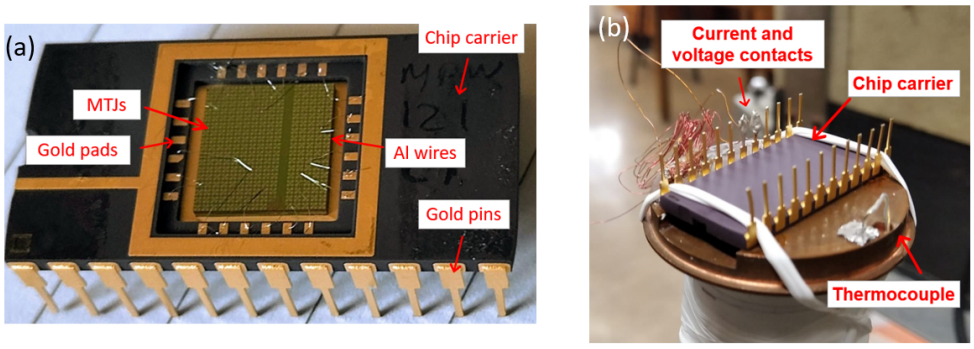

FIGURE 3.5: (a) Chip carrier connected to the MTJs contacts through aluminium wires. (b) Cryostat sample holder with the chip carrier placed on it to perform measurements.

smaller than the chip carrier, so that it can be placed downwards, as seen in Fig. 3.5(b). This is done so that the wires do not touch the sample holder, without the risk of breaking the bond. The sample is tied to the sample holder with Teflon tape, so it is properly fixed. In order to make electrical contacts with the chip carrier, the sample holder top face also contains thin copper wires. These are rolled around the chip carrier gold pins, which are then connected to the gold pads. Only two copper wires are used, since two-contact measurements were performed. These wires are wrapped around the cryostat arm, to minimize thermo-electrical effects in the measured bias voltage. To guarantee electrical contact between the pins and the copper wires, silver paintcr embeds them together. The sample holder also contains a small hole where an end of a thermocouple is placed, to measure its temperature. It is assumed, at the cost of a short approximation, that the temperature of the sample holder and the sample is the same.

The vacuum system is composed by a rotatory (primary) and a diffusion (secondary) pump. In order to perform vacuum, first, the rotatory pump is opened to the cryostat for about 15 minutes, to perform low-vacuum. After this, the primary pump is closed to the cryostat and the diffusion pump is opened to it, to perform high vacuum. The primary is connected to the secondary, to assist the vacuum. To lower the temperature inside the system, an helium compressor is turned on.

Measurement setup. A DC current is applied to the samples, supplied by the TIME ELECTRONICS 9818. The voltage created across the MTJs is measured by a Keithley 182 nanovoltmeter. Each of these devices is connected to one the copper wire in the sample holder. There is a Scientific Instruments INC Series 5500 Temperature Gauge, that ensures

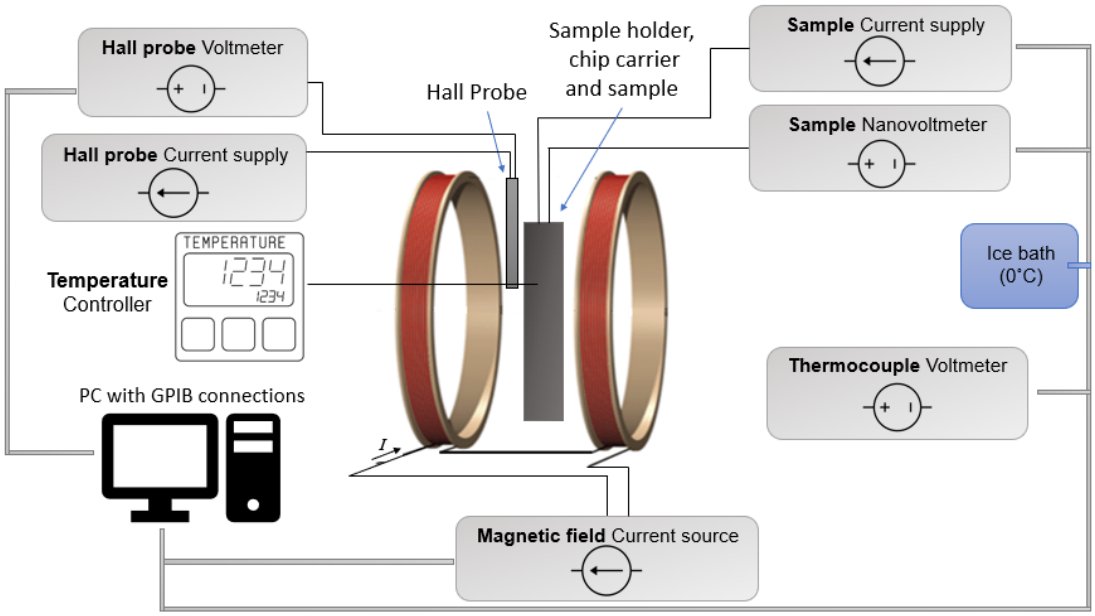

FIGURE 3.6: Schematic of cryogenic measurements setup.

a controlled temperature variation in temperature dependent measurements, and stabilizes the temperature. The sample temperature is then measured by a thermocouple, in which one end is fixed in the sample holder, and the other is coupled to an Agilent 34401A voltmeter, which measures the voltage generated by the thermocouple. The applied magnetic field is generated by Helmholtz coils, and a current about 1 mA is supplied to them by a KEPCO BOP 100-4M. A Hall probe measures the generated magnetic field and is supplied by a Keithley 225 current source. Finally, the voltage of the probe is measured by a HP 34401A multimeter. All the instruments are controlled in a personal computer, and are automatized through GPIB interfaces.

Chapter 4

Influence of Ta-doping on Tunnelling Processes and Power Generating Ability

This chapter is divided in three main sections: the first consists of the first characterization and comparison of control and Ta-doped junctions at room temperature; the second section presents a more extended temperature dependent analysis of the Ta-doped samples; in the third section the energy generation effect will be discussed.

4.1 Room temperature transport

The room temperature characterization of MgO-based MTJs is presented, for control and Ta-doped devices, as well as their comparison. The control/Ta-doped samples have a superficial area of 8x8 μm^2. These measurements were performed in the room temperature setup described in Chapter 3. The resistance area (RxA) product and resistance variation with applied magnetic field is represented in Fig. 4.1, for both control and Ta-doped junctions. The first conclusion one can take from the presence of the Ta particle layer in the middle of the MgO tunnel barrier, is the increase in RxA in both magnetic states. For the control sample, we obtained RxA_P = 3.5 MΩ μm^2 and RxA_{AP} = 7.4 MΩ μm^2, and in the Ta-sample RxA_P = 5.5 MΩ μm^2 and RxA_{AP} = 8 MΩ μm^2. These values are laid out in Table 4.1. This increase is also more pronounced in the P state, so that the difference between parallel and anti-parallel state is lower. In accordance to Fig. 4.1, this smaller difference

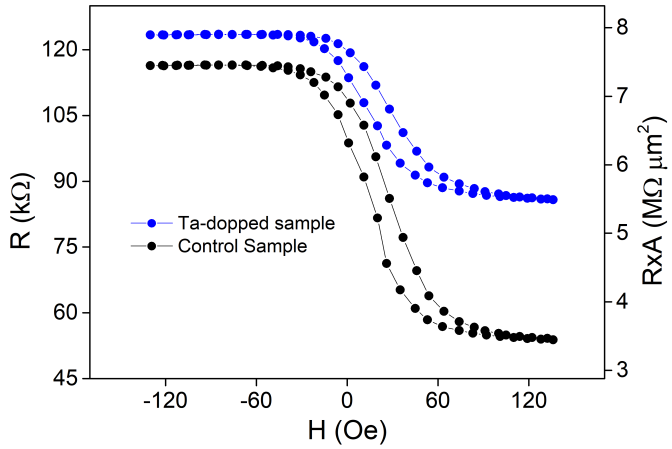

FIGURE 4.1: Resistance and resistance area product of 8x8 μm^2 control and Ta-doped junctions, as a function of the applied external in-plane magnetic field.

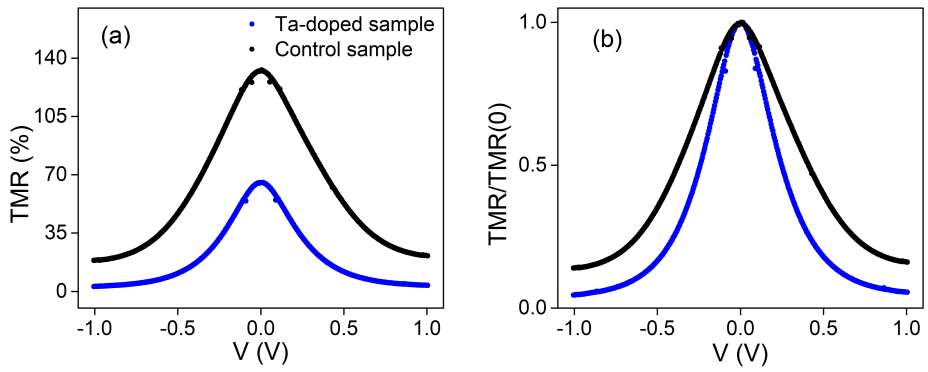

FIGURE 4.2: (a) TMR ratio and (b) normalized TMR ratio of a 8x8 μm^2 control and Ta-doped junctions, as a function of the applied external bias.

in resistance creates a very pronounced decrease in the maximum TMR ratio obtained, being of only 73% in this junction, while in the control junction the value is 163%.

In Figs. 4.2(a) and (b), the TMR and normalized TMR variation with bias voltage, respectively, is represented for both junctions. The first thing one notices, in accordance to what was expected from the RxA curve, is the substantive decrease of the maximum TMR ratio with the introduction of the Ta particles in the tunnel barrier. It is also clear that this doped junction presents a much faster decay in TMR with the increase in bias voltage. This behaviour is characterized by the figure of merit $V_{1/2}$ = 0.24 V, a much smaller voltage than for the control junction $V_{1/2}$ = 0.41 V.

The current-voltage curves of the control and Ta-doped samples are represented in Fig. 4.3, at RT. The curves in the parallel and anti-parallel states of each sample seem to overlap in the first graph, but in the second graph which represents the curves between

Sample	RA_P ($M\Omega\mu m^2$)	RA_{AP} ($M\Omega\mu m^2$)	TMR (%)	$V_{1/2}$ (V)
Control	3.5	7.4	163	0.41
Ta-doped	5.5	8	73	0.24

TABLE 4.1: Representative values of the main characteristic factors of control and Ta-doped samples.

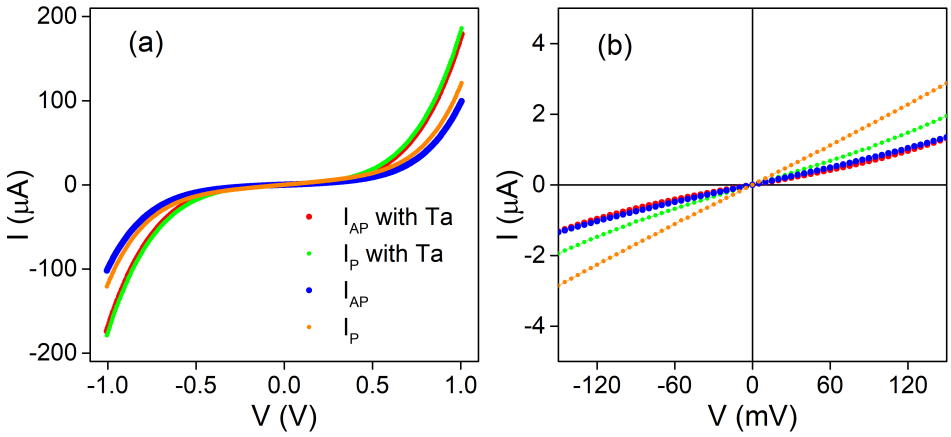

FIGURE 4.3: (a) Current-voltage curves for both control and Ta-doped junctions, at 300 K. (b) Zoom in the curves from (a), between -130 and 130 mV.

-0.15 and 0.15 V, we see that they do not. This is due to the fact that these samples are highly resistive, as we have mentioned. We also can see that, above ≈0.5 V, the current in the Ta-doped junctions reaches a higher value than the control samples, which must mean that the conductance in this sample has increased more significantly with increasing bias. The curves were fitted with the Simmon's Model equation for intermediate bias (Eq. 1.7), referenced in Section 1.4 from Chapter 1, and the obtained parameters are shown in Table 4.2.

Sample	ϕ_{AP} (eV)	ϕ_P (eV)	t_{AP} (nm)	t_P (nm)
Control	1.22	1.29	1.86	1.79
Ta-doped	1.23	1.25	1.97	1.77

TABLE 4.2: Obtained parameters using the Simmon's model to fit the current-voltage curves, concerning Fig. 4.3(a).

In Fig. 4.4 is represented the conductance, $G = dI/dV$, of the control and Ta-doped samples, at room temperature (RT). At zero bias, the conductance is higher for the control samples, but quickly, as the bias is increased, the conductance of the Ta-doped sample surpasses it, so there is a faster increase in conductance in this sample.

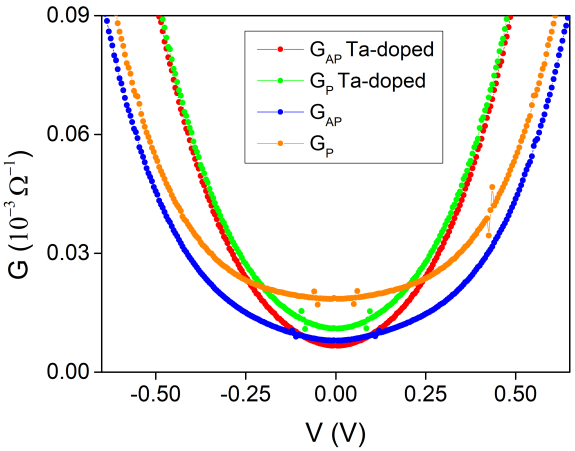

FIGURE 4.4: Conductance in P and AP state for both control and Ta-doped junctions, at 300K.

From the behaviours we have observed, it is clear that the presence of the paramagnetic particles in the MgO barrier has a major influence in the physical properties of tunnel junctions. We observed that the resistance is enhanced, indicating that the Ta particles create difficulty to the tunnelling electrons and, at the same time, TMR decreases and the dependency on bias voltage is much larger, which means that somehow, the particles act as an extra spin-independent conductance channel. These behaviours seem contradictory, so the origin behind them must be different.

One possible explanation is that the Ta particles layer causes an increase in the barrier thickness, which may cause a significant increase in the resistance. According to Simmon's model [11], the tunnelling current at low bias (V $\approx$ 0), is given by:

$$I = k_0 k_1 \frac{A exp(-k_1 t\sqrt{\phi})}{2t} V, \tag{4.1}$$

where the parameters are the same as described in Section 1.4 from Chapter 1. From the previews expression we can write the resistance (R) in the following way:

$$R = \frac{V}{I} = \frac{1}{k_0 k_1} \frac{2t}{A} exp(k_1 t\sqrt{\phi}). \tag{4.2}$$

This equation shows that, for small bias, the resistance of an MTJ follows Ohm's law, increasing exponentially with the barrier thickness and the square root of the barrier height. This indicates that the introduction of the Ta particles can lead to a large increase in the MTJ resistance. Considering the experimental increase in resistance from the samples, we obtained for the P state: $\frac{R_{Ta-doped}}{R_{Control}} = 1.57$.

Using Eq. 4.2 to determine the theoretical ratio between resistances, we obtain the expression:

$$\frac{R_{Ta-doped}}{R_{Control}} = \frac{t + t_{Ta}}{t} exp(k_1 t(\sqrt{\phi_{Ta}} - \sqrt{\phi}) + k_1 t_{Ta}\sqrt{\phi_{Ta}}), \tag{4.3}$$

where t and ϕ correspond to the thickness and barrier height of the control sample, and $t^{'} = t + t_{Ta}$ and ϕ_{Ta} are the thickness and barrier height of the Ta-doped sample. Using the values for barrier thickness and height obtained from the Simmon's model fit for intermediate bias (Eq. 1.7), we obtain $\frac{R_{Ta-doped}}{R_{Control}} = 1.51$.

We thus find that the model and experimental values of the resistance increase are remarkably similar, with a percentage error of $\frac{R_{model} - R_{experimental}}{R_{model}} \times 100 = 4\%$. This indicates that the introduction of the extra Ta layer does account for the enhancement in the junction's resistance. The origin of the TMR decrease will be further investigated in the next sections.

4.1.1 Resonant tunnelling through trapping states

Figure 4.5 represents the normalized second derivative of the current (d^2I/dV^2 or dG/dV) of the control sample, in the AP and P states. This measurement was performed in the room temperature setup described in Chapter 3, which showed significant noise, and most of the fine structure anomalies were masked by it. Nevertheless, it is still possible to identify an anomaly around 0.45 V, that is present in both magnetization states. This anomaly comprises a peak followed by a valley, with about the same intensity in both states. This said, we can first affirm that this anomaly represents an elastic tunnelling process, namely trap assisted tunnelling, and that its origin is in the insulating barrier or near the FM/IN interface. This trap could be any kind of vacancy, dislocation of step edges in the barrier structure. The shape of the feature in both positive and negative voltages is very similar, which indicates that they have origin on the same trap. Their intensity is also very similar, which indicates that the barrier is symmetric.

The same feature was not observed in the Ta-doped samples. One of the reasons might be that the feature was not strong enough to be noticed amongst the noise. We also know that the electronic properties of oxide materials are affected by the presence of any kind of impurities or defects, locally perturbing the lattice. That said, another possible explanation is that the presence of the Ta particles affects the electronic configuration of the tunnel barrier, and the traps that originated the feature in the control sample are not formed in

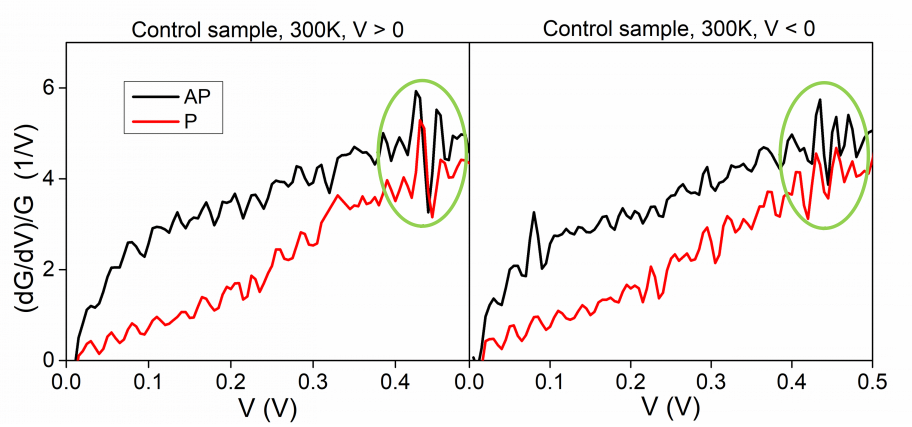

FIGURE 4.5: IETS spectra (a) V $>$ 0 V and (b) V $<$ 0 V, in the parallel and anti-parallel state of the control sample, at room temperature.

the doped samples. From this we can take that the tunnel barriers of the control samples also contain certain defects, which in this case led to the formation of a resonant trapping state.

4.2 Temperature dependent transport

In this section will be presented the temperature dependent analysis performed on Ta-doped MTJ samples. We performed the first measurements in a 18x18 μ^2m sample, which we shall identify as Sample 1.

4.2.1 Magnetic field dependency

The resistance area product (RxA) and TMR(H) transfer curves were measured by applying an external magnetic field in the direction of the easy magnetization axis of the MTJs, and varying its intensity and sign, for doped magnetic tunnel junctions. In Fig. 4.6 are represented the curves for the first sample which was measured (Sample 1), of area 18x18 μm^2. These loops were measured at low bias, with an applied current of 0.1 μA, and temperatures from 320 to 28 K. At room temperature, a lower RxA product was observed for both states, with a difference between the resistance in the parallel and anti-parallel states much smaller, which led to a smaller maximum TMR ratio. As the temperature is decreased, the RxA product is enhanced, an effect particularly important for the anti-parallel state, leading to very large TMR ratios, as can be seen in Fig. 4.6(a). The TMR ratio in the doped junction increases from 65% at RT, to 185% at 28 K. We find full saturation of the magnetic states for a magnetic field of 100 Oe at all temperatures. This means

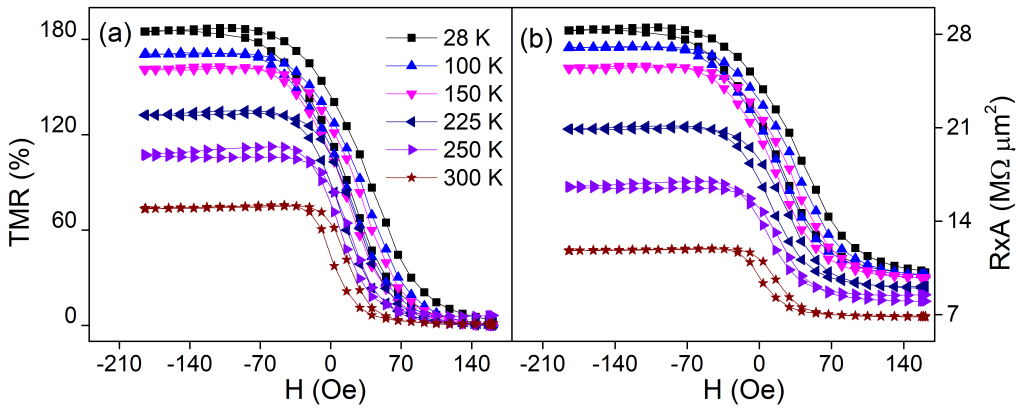

FIGURE 4.6: (a) TMR ratio and (b) Resistance times area product, of Sample 1 (Ta-doped junction), in function of applied external in-plane magnetic field, for different temperatures.

that there is full parallelism (positive field) and anti-parallelism (negative field) between the pinned and the free layer.

4.2.2 Bias voltage dependency

The current-voltage curves obtained for Sample 1 can be seen in Fig. 4.7(a). The curves follow the expected behaviour, which can be fitted with the Simmon's model, with the non-linear I-V behaviour, characteristic of electron tunnelling. We notice that, for the same value of applied bias, the current is higher at 300 K, which indicates a lower resistance at this temperature. Concerning the TMR variation with applied external bias, for different temperatures, we conclude that, as temperature reaches cryogenic values, an increase in the TMR at 0 V is achieved, as can be seen in Fig. 4.7(b). To characterize this dependency with increasing bias, the figure of merit $V_{1/2}$ was determined for each temperature. The value at 28 K is $V_{1/2}^{28K} = 97$ mV and $V_{1/2}^{300K} = 118$ mV, at room temperature. The variation from 28 K to 300 K is only 21 mV, so one can say that this parameter has a very weak dependency on temperature. This indicates that, although the TMR suffers a large increase with decreasing temperature around zero bias, the dependence on external applied bias is very strong, and the effects that cause the reduction of the TMR are still present even at low temperature.

We observe that, for increasing temperature and bias, there is a significant detriment in TMR. With the decreasing temperature and bias, TMR is enhanced.

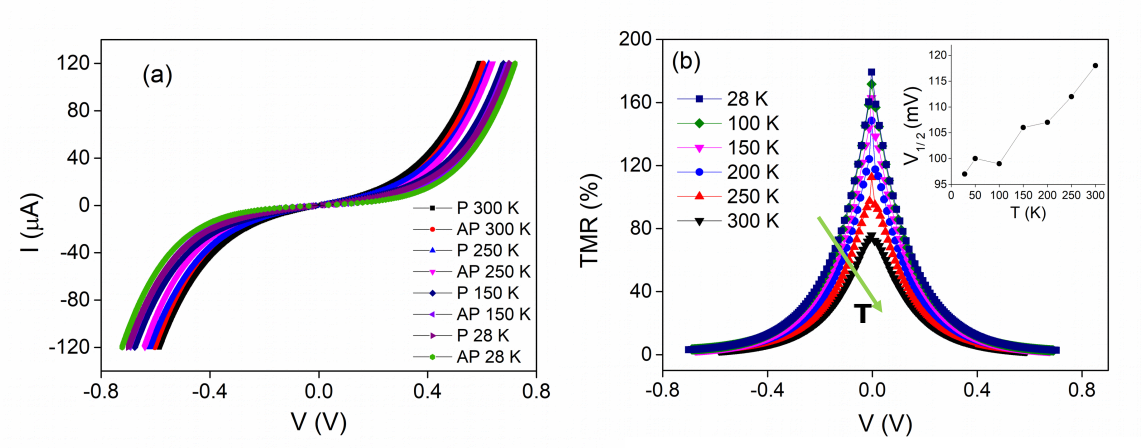

FIGURE 4.7: (a) TMR ratio as a function of applied external bias voltage, for different temperatures and (b) Current-voltage curves for 28 and 300 K, in AP and P states, of Sample 1. The inset on (b) represents the figure of merit $V_{1/2}$ of the curves of each temperature.

4.2.3 Conductance bias and temperature dependence

In this section will be discussed the bias dependence of the conductance in doped tunnel junctions, at different temperature between 28 and 300 K, for the P and AP states. The conductance has been numerically calculated from the obtained I-V data (G = dI/dV), as a function of the applied bias voltage, and the results are depicted in Fig. 4.8 for 28 and 300 K.

The existing models for elastic tunnelling, which predict a parabolic like behaviour, were applied to the curves considering only higher voltage ($\gtrsim$ 0.4 V). The models showed to be a good fit to the curves, since they do show a parabolic behaviour. But for voltages below $\pm$ 0.4 V, the variation of the conductance is much slower, especially for 28 K (Fig. 4.8(a)), and the fit is not adequate. This indicates that elastic tunnelling is not the main tunnelling mechanism in these junctions at low bias, or that it is suppressed by other effects. We must notice that these samples have very large resistance, with a RxA product in the order of M$\Omega\mu$m^2. This is not a favourable factor in the performance of the measurements, since it can cause much noise and hide anomalies in the conductance. We observe that the variation of G around 0 V is much faster at 300 K, which is in accordance to the lower maximum TMR ratios achieved for higher temperatures.

We also find a very symmetrical shape of the curve around zero bias. When there are asymmetries, it is usually an indication of a difference in the quality of the upper and lower CoFeB/MgO interfaces, which can be expected, since the particles are introduced in the middle of the MgO layer. Another thing to notice is that no zero-bias anomaly (ZBA)

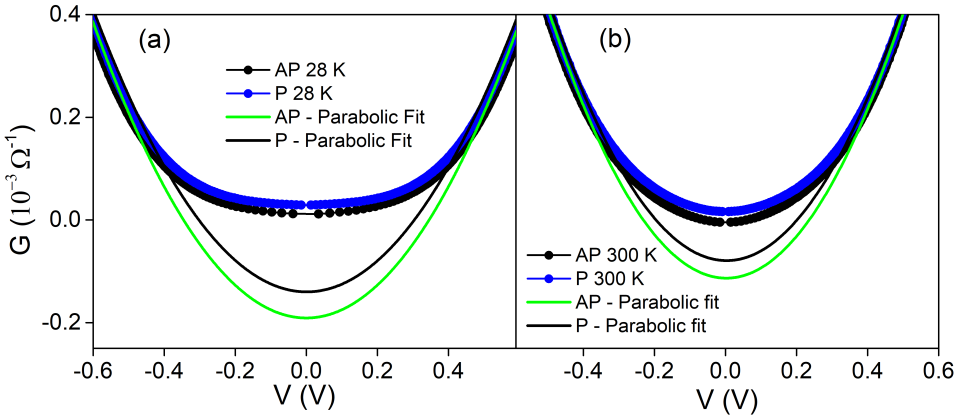

FIGURE 4.8: Conductance as a function of applied bias voltage for Sample 1 and respective parabolic fits at (a) 28 K and (b) 300 K.

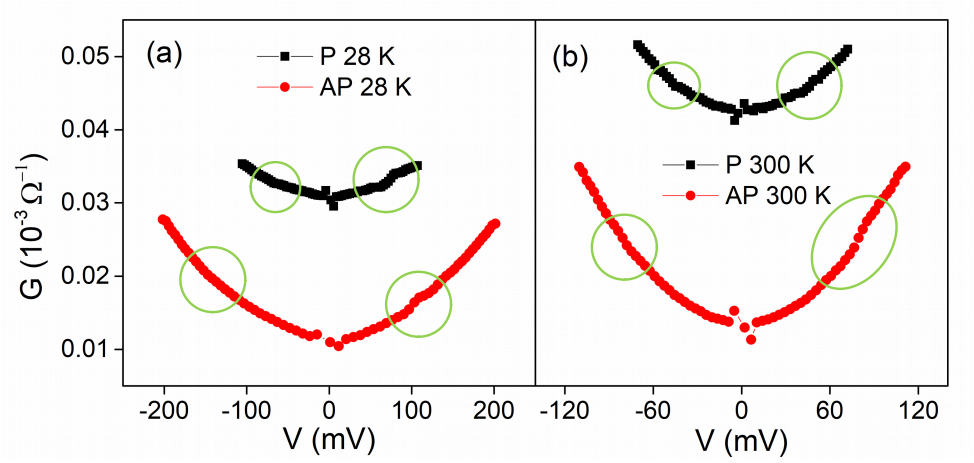

FIGURE 4.9: Parallel and anti-parallel conductance of a Ta-doped junction, at (a) 28 K and (b) 300 K. The green circles mark the visible anomalies in each branch.

is observed in our data. ZBA usually results from inelastic excitations, such as magnons, as discussed earlier in Chapter 1. But neither in the parallel or anti-parallel states there is evidence of this effect.

Measurements of conductance at low bias were also performed in order to determine trapping states in the junctions. For higher bias it was not possible to do this kind of characterization, since these samples are extremely resistive, and the noise is much larger than the features one wants to see. In Fig. 4.9, the conductance at low bias is represented for Sample 1. One easily observes the anomalies marked by the green circles in the figure, which are more pronounced at 28 K in the AP alignment, but reproduced at all temperatures, namely at 300 K.

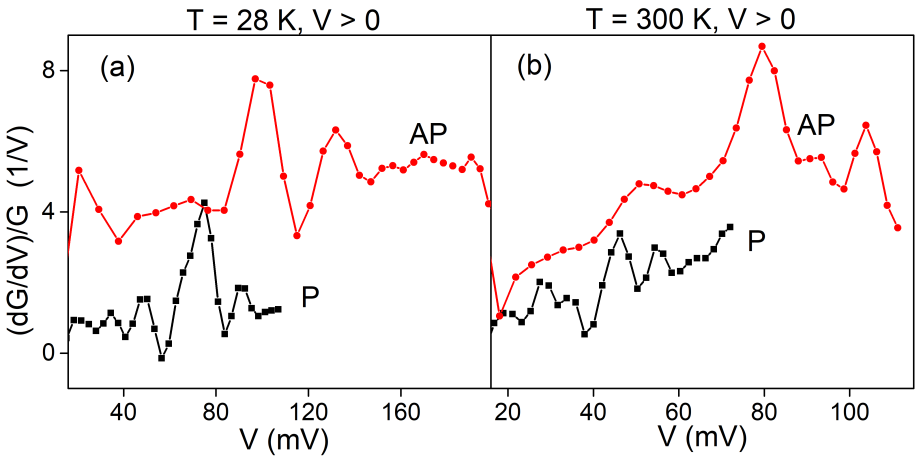

FIGURE 4.10: IETS spectra for the parallel and anti-parallel state of a Ta-doped junction, at (a) 28 K and (b) 300 K.

The origin of these anomalies might have to do with the structure of the CoFeB ferromagnets, or with the MgO tunnel barrier. If the ferromagnets majority spin DOS is diminished around the Fermi energy, due to the increase in voltage, one would expect a significant dip in the P state, but more subtle in the AP state. If the cause is related with the tunnelling probability in MgO, the dip in both states should be the same. Or, said in another way, the ratio between the dip in dI^2/d^2V and dI/dV should be similar. It is clear that the anomalies are more pronounced for positive bias voltage, which indicates an asymmetry in the tunnel barrier, which is expected since the introduction of the particles affects the way MgO grows below and on top of them.

In the IETS spectra represented in Fig. 4.10 we are able to see this anomaly more clearly. One notices that it originates a peak followed by a valley, which labels an anomaly caused by trap assisted tunnelling. This is a kind of elastic trapping process that occurs at the insulator barrier, or near the ferromagnet/insulator interface. An elastic process should not be strongly dependent on temperature, and we actually notice that these features do not change significantly with temperature. It is interesting to know if this is an anomaly created by the presence of Ta particles, or if it is due to defects in the barrier itself.

Next, we shall consider the T-dependency of the conductance, which is represented in Fig. 4.11(a), for both parallel and anti-parallel states, at zero bias, for Sample 1. In both curves we observe an increase in the conductance with increasing T, i.e. an insulator-like behaviour. The enhancement in the conductance is quite strong. Following the direct tunnelling model, G_P should decrease with temperature, in contrast to what these results

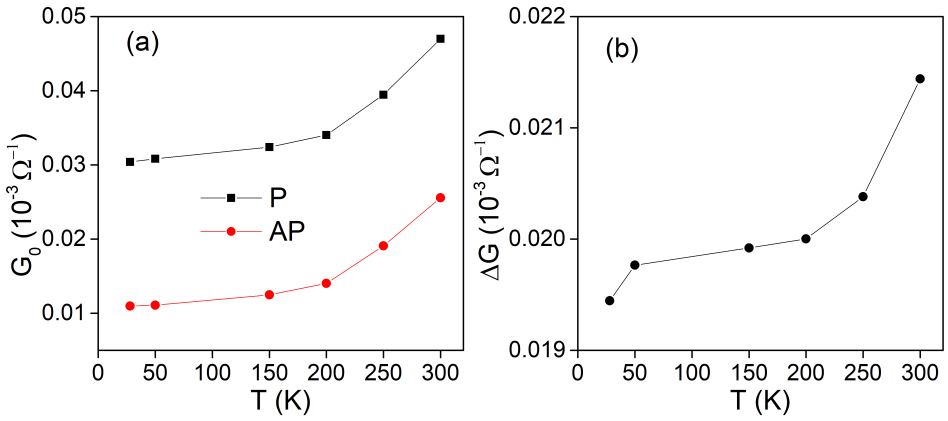

FIGURE 4.11: (a) Conductance in parallel and anti-parallel state and (b) $\Delta G = G_P - G_{AP}$, as a function of temperature for the Ta-doped sample.

show. Such a large increase is an indication of some temperature-dependent transport channel. One possibility is spin-independent tunnelling via hopping sites in the barrier, phonon assisted tunnelling and electron scattering on impurities created at the FM/TB interface [44], as discussed in Chapter 2.

From Fig. 4.11(b) we see that the difference between conductance in the P and AP state, $\Delta G(T) = G_P - G_{AP}$, is increasing with temperature, which means that the rate of increase of G_P is higher than for G_{AP}. This is evidence of a spin-conserving tunnel assisted mechanism [45]. From this behaviour we can also exclude the model of excitation/absorption of magnons [24], that predicts a decreasing ΔG, consistent with spin-flip transport mechanisms, that usually contribute more to G_{AP} than to G_P. As has been mentioned before, ZBA is also a consequence of this type of mechanism. Both the absence of ZBA in these samples and the variation of conductance with T suggest that magnon-assisted tunnelling is not one of the main mechanisms observed in the Ta-doped junctions.

4.2.4 TMR and resistance variation with temperature

Concerning Sample 1, the maximum TMR ratio and the electrical resistance R(T) in both P and AP states, for each temperature, are shown in Figs. 4.12(a) and (b), respectively. The measurements were performed in a temperature range between 22 and 320 K. The variation of TMR with temperature displays an interesting behaviour. At higher temperatures a fast decay of TMR is observed, compared to what is expected from usual MTJs. But more intriguing is the behaviour at very low temperature: a strong enhancement of TMR is observed in this junction at temperatures lower than 30 K, but no definitive explanation

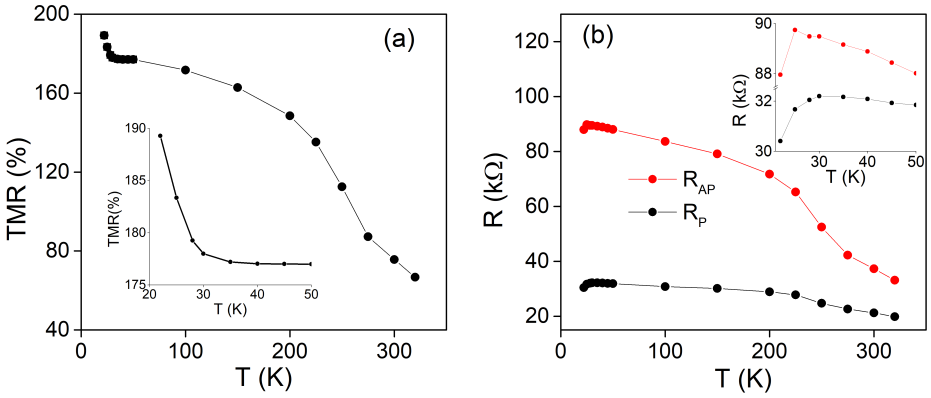

FIGURE 4.12: (a) TMR ratio T-dependency and (b) Parallel and anti-parallel magnetization state resistance T-dependency of Sample 1.

was found for this behaviour. Nevertheless, we should mention that a behaviour similar to this was found in Ref. [37]. The same kind of rapid growth at temperatures below 50 K was observed and attributed to Coulomb Blockade. It was considered that the thermal energy is much lower than the charging energy of the particles, so that direct tunnelling is suppressed, and only inelastic co-tunnelling is allowed, diminishing the conductance, and enhancing the TMR ratio. However, unlike in our results, the resistance continues to increase at these temperatures.

From the behaviour represented in Fig. 4.12(b) we can tell that, for temperatures higher than 30 K, we find a negative dR/dT, which is indicative of an insulator-like behaviour. We notice that, as temperature increases, the absolute value of the derivative increases, indicating a strong enhancement of the tunnelling current. For very low temperatures, we find a positive dR/dT, characteristic of a metal-like behaviour.

Magnetic disorder, which increases with temperature, is responsible for a decrease in R_{AP}, but causes the increase in R_P. Thermal excitations, on the other side, cause the decrease of R in both sates [46]. In these results we do see a decrease in resistance for both magnetic sates, in accordance to the behaviour obtained in conductance, which means that thermal excitations must be more influential in this effect than magnetic disorder.

A set of criteria was determined in the 1960s and 1970s to identify single-step elastic electron tunnelling in superconductor-insulator-superconductor tri-layers, called the Rowell criteria [47]. Among those, one that applies to non-superconducting electrodes is that there should be a weak insulating-like dependence of the conductance or resistance with temperature. In these graphs we do find a behaviour similar to this, which tells us that, despite the existence of other transport channels, direct tunnelling is still present and

accounts for a large part of the tunnelling transport. In Ref. [12], it was concluded that an insulator-like behaviour rules out the possibility of pinholes in the barrier. This indicates us that, other than the paramagnetic impurities embedded in the TB, the MgO has good quality.

4.2.5 Discussion

We have observed a strong reduction of TMR with increasing bias and temperature and, by the variation of the resistance as a function of temperature, which presents a weak-insulator like behaviour, we see that direct tunnelling modulates the general behaviour of the MTJ. At the same time, we determined that at low bias the main mechanism contributing to the conductance should not be direct elastic tunnelling. Concerning the variation of conductance with temperature, we found an increase on both magnetic states, even more prominently in the parallel state. This, of course, caused a strong increase of the overall conductance with temperature. Among inelastic mechanisms, magnon excitation does not appear to have a major influence in the tunnelling, since according to the model developed by Zhang et al. [24], G_P should decrease due to the absorption of magnons in the FM/TB interfaces. Plus, no ZBA effect was observed in the studied junctions. Several other models were proposed to explain the behaviour of TMR and conductance with different mechanisms in tunnel junctions. We shall analyse some that might fit the characteristics of our junctions.

Zhang and White [26] studied the bias dependency of the TMR in MTJs, and concluded that the basic Julliere's model which considers only spin-dependent direct tunnelling was insufficient to explain the behaviour of these devices. The authors considered both spin-dependent direct tunnelling and another spin-independent tunnelling mechanism. Even though these barriers were not purposely doped with impurities, the inherent defects created upon the fabrication of the devices had enough influence to consider the extra conduction channel. The studied tunnel junctions present strong bias and temperature dependencies. The model considers the existence of defect states in the tunnel barrier, whose electrons will be excited by thermal activation processes, creating available states for two step tunnelling. Electrons could be excited either by temperature increase or through hot electron impact. Since these defects are not polarized, the process becomes spin-independent, generating a spin-independent current that does not contribute to TMR enhancement. The voltage dependence was explained in terms of Fermi-Dirac functions,

that indicates that the density of available states increases exponentially as the energy levels increase. So, two step tunnelling is intensified with increased bias. Considering the application of this model in our system, Ta particles can be looked at as trapping states in the barrier, since they have such a small size and concentration. With the increase in temperature, Ta particles are excited, originating available states for the two step tunnelling, creating a spin-independent current, this way decreasing TMR.

Shang et al. [33] also developed a model in which the conductance can be expressed by Eq. 2.2, as discussed in Section 2.4. There is a term, G_{SI}, that is unpolarized and dominated by hopping through defects in the barrier, and therefore, spin-independent. This parameter is enhanced with increasing temperature and does not depend on the relative orientation of the magnetization. The direct elastic tunnelling term G_T will increase the conductance with the enhancement of temperature. On the contrary, the polarization contributes with an opposite slope in the conductance. For G_P, this gives a negative contribution from the direct tunnelling term, and a positive contribution from the hopping term, which results in a small variation of the conductance with temperature, in the parallel state. Actually, a slight increase in $G_P(V = 0)$ is usually an indication of good quality MgO tunnel barrier [31, 48]. So, finding a large $G(T)$ increase may be an indication of the presence of the Ta paramagnetic impurities, which obviously decrease the quality of the barrier.

Both the above exposed models consider that the presence of defects or impurities states in the barrier create extra conduction paths for electrons to tunnel, which contribute to the overall conductance by increasing it.

There are also reports [49–51] that specifically studied the effect of introducing non-magnetic impurities in the AlOx tunnel barrier, and which results are very similar to what we have observed in our junctions. The observed behaviours were explained considering an elastic contribution from impurity-assisted tunnelling: Impurities in the barrier act as trapping states, which create extra conduction channels for electrons, decreasing the resistance and the TMR.

In Ref. [50], Dy- and Gd-doped Al_2O_3 MTJs were studied, and at low temperature and bias, the TMR stayed unaffected, comparing to similar control junctions. By increasing T and V, the TMR reduces quite faster than in the control junctions. The same behaviour is also reported in Refs. [49, 51]. A theoretical explanation is presented by Bratkovsky [10] and also Tsymbal et al. [52]. In the latest work, a rapid drop of TMR as a function of T

and V is observed in amorphous barriers doped with non-magnetic particles. It is stated that the higher the impurity concentration, the more localized electronic levels close to the Fermi energy level are created, forming highly conducting channels across the insulator. Both TMR and FM polarization decrease rapidly, as impurities with energy near the Fermi energy of the insulator create a large number of electronic levels, forming highly conducting channels in the insulator. These electronic states extend from one side of the barrier to the other, dominating the conductance, hybridizing with states from the FMs. Since tunnelling through impurity levels in the barrier is governed by the overlap of unpolarized impurity levels and electrode wave functions, the effective polarization is reduced [10]. In summary, the mixture of spin-independent impurity states with spin dependent wave functions of tunnelling electrons reduces the spin polarization and drops TMR. We should notice that these considerations are given in light of amorphous barriers, where the existence of conductance paths due to impurities is well established [53]. Nevertheless, one could consider the same explanation, regarding only the electrons that are transmitted in MgO tunnel barriers, in accordance to the MgO spin-filtering mechanism. Concerning the junctions studied in this thesis, the Ta particles could break the spin-filtering mechanism of the MgO, creating conductive paths for all electrons.

At this point is clear that the effect of the introduction of Ta particles is in accordance to the existing impurity assisted tunnelling models, and accounts for the strong dependency on bias and temperature that is observed in TMR. The strong bias dependency that is predicted by this tunnelling mechanism, also agrees with the small variation of the figure of merit $V_{1/2}$ that was obtained, since even at high temperatures, there is a strong variation of TMR with bias.

Concerning the observed G(V) behaviour, the parabolic fits showed that, for low voltage, the direct tunnelling model is not followed. The variation of G_0 with temperature is in accordance to this result, since it shows an increase with increasing temperature, and the direct tunnelling model expects a decrease. We can then affirm that some temperature-dependent transport mechanism is responsible for the tunnelling at low bias. Adding to that, we find an increase in ΔG, which suggests a spin-conserving tunnelling mechanism. The previous models are also in agreement with this behaviour, since they predict an enhancement of the conductance with temperature. We observe in our G(T) graphs that, for both G_{AP} and G_P, the conductance increases with temperature. This could indicate that hopping is one of the most significant tunnelling mechanisms in our junctions, surpassing

the effect of direct tunnelling. We should note that hopping is less likely in MgO barriers than AlOx, due to the smaller density of localized states. That said, in our junctions the Ta particles might create these localized states and increase the probability of this mechanism. Another possible explanation for the growth of ΔG is phonon absorption/emission. This is also a spin-independent mechanism and there is spin conservation. When the MTJ structure is annealed, oxygen atoms, that might have oxidated the bottom FM layer, diffuse from the FM to the tunnel barrier, making it harder to have magnon absorption and lowering the phonon energy spectrum of the FM/TB, so it is easier to activate phonons. Phonons are also thermally excited [45], so their contribution becomes larger at larger temperatures.

4.3 Energy generation

To study the effect of power generation, we look deeper into the offsets, ΔV, of the measured current-voltage curves. Figure 4.13 shows the current-voltage curve for Sample 1, in a smaller range, at 28 and 300 K.

Although one would expect no current offset for 0 V, all temperatures depict an offset in the I-V curves. These dependencies are in agreement with what would be expected for the effect. In fact, in accordance to [13], the largest power generation is expected in the AP configuration, as discussed in Section 2.6 from Chapter 2. It would also be natural to see an enhancement of the effect at cryogenic temperature since quantum effects are

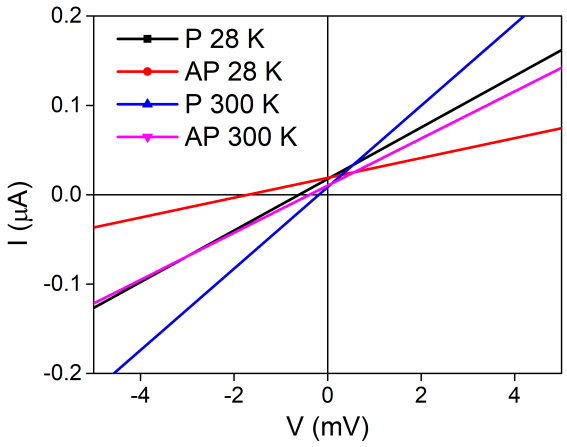

FIGURE 4.13: Sample 1 current-voltage curves around 0 V, in P and AP states, at 28 and 300 K.

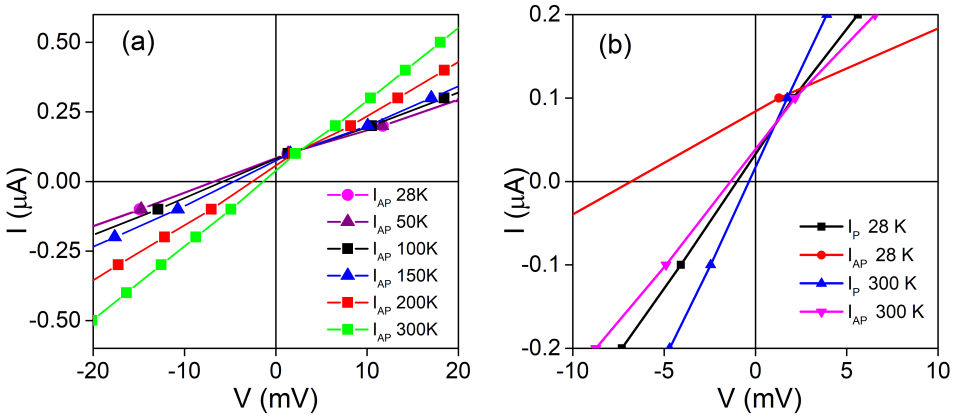

FIGURE 4.14: (a) Current-voltage curves at different temperatures and (b) Current-voltage curves in the P and AP state, at 28 and 300 K, of Sample 1'.

enhanced at lower temperatures and this Ta-doped MgO barrier device is the first with this configuration, so the effect is not tuned to work at room temperature.

After a few weeks, Sample 1 was measured again to study the reproducibility of the results in the same sample, and determine if its behaviour had changed and how. We found that it presented different characteristics, namely lower resistance values in the AP state. We shall identify the measurements performed under these conditions by referring to Sample 1'. For Sample 1', a RxA product of 2.59/1.0 M$\Omega\mu$m^2 at 28 K and 1.19/0.67 M$\Omega\mu$m^2 at 300 K, in the AP/P configuration, was obtained (R of 79.96/31.02 kΩ at 28 K and 36.75/20.69 kΩ at 300 K, in the AP/P configuration).

In Fig. 4.14(a), the current in Sample 1' in the AP state around the point (I,V) = (0,0) is represented in a range of temperatures between 28 and 300 K. We see that, for the entire range of temperatures, ΔV is enhanced as temperature is decreased (see also Fig. 4.15). This behaviour is in accordance to what is expected, considering that, as temperature diminishes, the resistance is increased, and the offset may be affected by that. However, we also notice that the difference between offsets in the AP and P state seems to be larger for the curves that correspond to 28 K than 300 K, which could be an indication of the presence of the energy harvesting effect. To analyse the data more precisely, the offset ΔV as a function of temperature was traced, for both sample 1 and sample 1', and is shown in Fig. 4.15. The ΔV variation with temperature seems to follow a similar behaviour in both samples, although in Sample 1' the values are much higher concerning the AP state. This behaviour also mimics the T-dependency of the resistance shown in Fig. 4.12(b) (R vs T), which indicates that this offset is related to the variation in the resistance, which

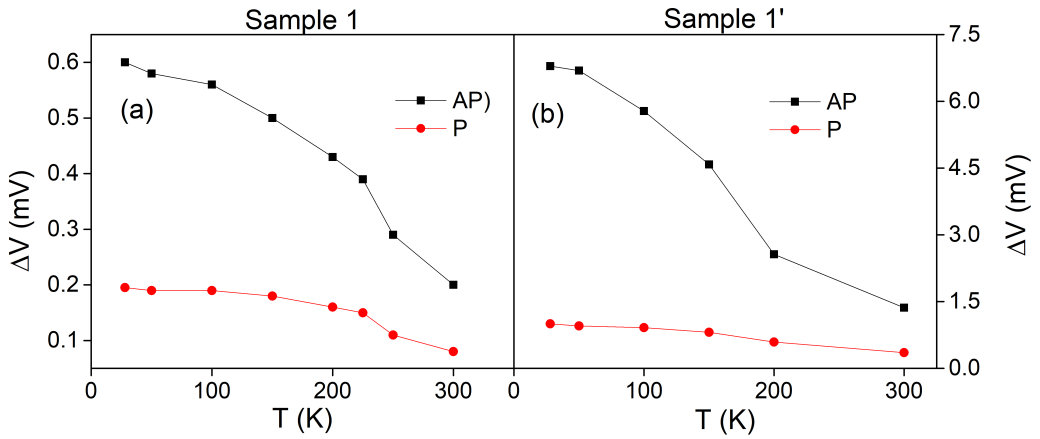

FIGURE 4.15: Offset as a function of temperature in (a) Sample 1 and (b) Sample 1'.

of course affects the measurements. However, given the large offsets obtained in Sample 1', these values seem to have origin in the power generating effect. But this solely is not a strong enough evidence, as the variable we are measuring is of very small magnitude, and is extremely conditioned by the measuring conditions.

This temperature dependence of the offset could be due to measurements artefacts, namely small currents from the setup devices. The magnetization state dependence could be related with the fact that these currents depend on the device resistance, which is influenced by the magnetic state. To test this possibility and unveil the nature of the obtained offsets in the current-voltage curves for each measured MTJ, studies were performed with a resistance box. The box was connected to the system, and I-V curves were measured, applying a resistance that corresponds to values of P and AP resistances of the MTJ at certain temperatures. For each resistance, three curves were measured using the same scale and step, so that the measurements conditions were reproduced. The results obtained through these measurements are strictly due to the resistance that is being applied and how the system replies to it. So, we know that there are no effects from the MTJs contributing. In Fig. 4.16(a) are represented the offsets obtained from the measures using the resistance box, as well the offsets from Sample 1 and Sample 1', as a function of the resistance. The same data is represented in Fig. 4.16(b) in a logarithmic scale.

From the graph on the right, we determine that the offsets corresponding to Sample 1 are lower than the resistance box. Would there be any thermal fluctuations rectification, we would expect to see a larger offset than the one caused solely by the resistance applied to the system. This is an indication that in Sample 1 no significant effect was observed. Nevertheless, we would also expect that this offset was the same value as the one in the

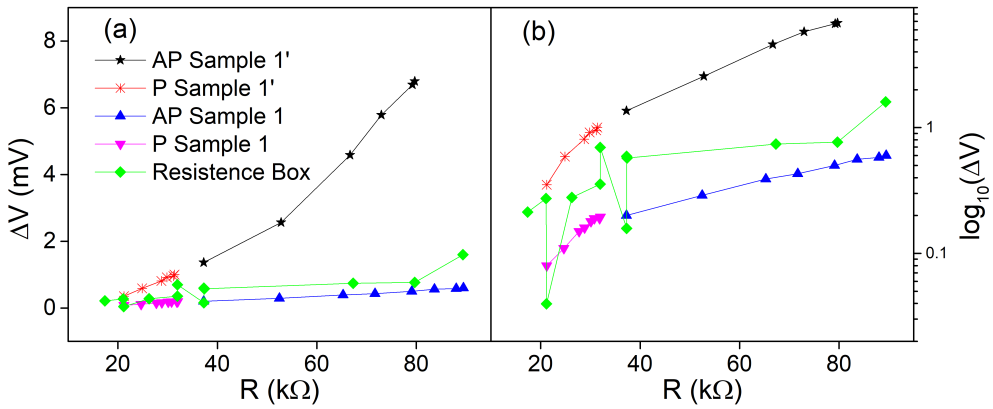

FIGURE 4.16: (a) Offset as a function of resistance in Sample 1, Sample 1' and the resistance box. (b) Logarithmic representation of the data from (a).

resistance box. From the jumps we see in the offsets of the resistance box, we may also assume that there is an uncertainty associated to these measurements.

The larger rate of increase we observe in the data from Sample 1' seems to indicate that the effect of thermal rectifications is present in the junction. However, the graph on the right unveils a similar growth tendency with R in all the samples. Besides that, even the parallel state exhibits a tendency that is followed by the AP state. Recalling the discussion of the effect in Section 2.6 from Chapter 2, one of the conditions for the reproduction of the effect is an asymmetric energy profile, that is obtained only in the AP state. So, were the effect present, we should only see it in the anti-parallel state.

After all these considerations, we cannot definitely affirm that the effect was reproduced in the junctions studied in this thesis. In the article from Ref. [13], it is affirmed that this effect was reproduced only in 1 out of 200 tunnel junctions. This number is a reflection of the lack of reproducibility still associated to this effect. In this thesis only a few MTJs were characterized, both due to the setup and time limitations. We conclude that further studies would be necessary to be able to study a larger number of devices and corroborate the results, or have the opportunity to reproduce the desired effect with confidence.

4.3.1 Effect Reproducibility

Here we present the results that were obtained in two other MTJs that were studied. In total, three different samples were measured as a function of temperature: a 18x18 μm^2,

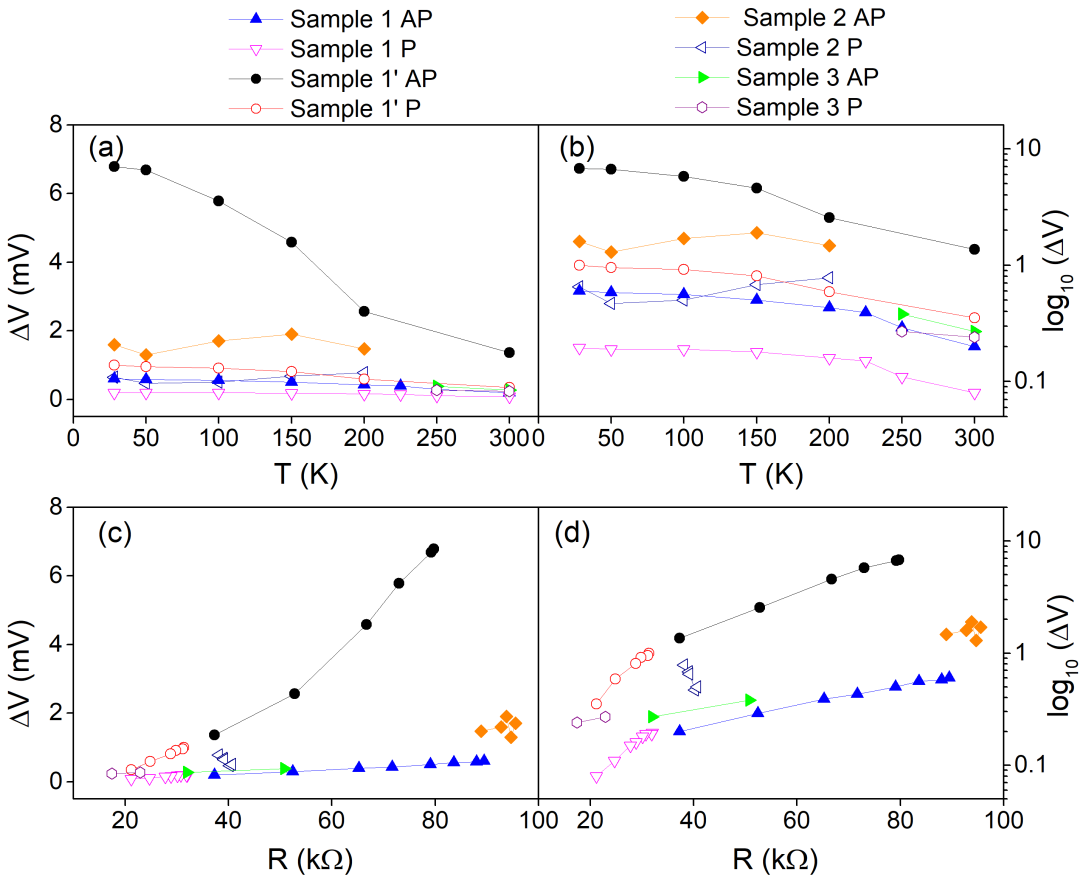

FIGURE 4.17: Offset in Sample 1, 1', 2 and 3: (a) in linear scale and (b) in logarithmic scale, as a function of temperature; (c) in linear scale and (d) in logarithmic scale, as a function of resistance.

being that this one was measured two times (Sample 1 and Sample 1'), a 14x14 μm^2 (Sample 2) and a 20x20 μm^2 (Sample 3). The offsets obtained in the current-voltage curves are shown in Figs. 4.17(a) and (c), as a function of temperature and the resistance of the sample, respectively, and in logarithmic scale ((b) and (d)).

We see that the behaviours between the samples are very different. Not all of them follow a linear increase with resistance, and the values of the offset for similar resistance values can be quite different. What we take from this is that the samples, which were fabricated in the same series with the exact same conditions, do not present a constant behaviour, which indicates that different variables are affecting the results. As already mentioned, the conditions of the setup measurements can also influence the results, given that the quantity that we are measuring is small. All the measurements were performed in different days, throughout the course of a few weeks. However, given that even the logarithmic behaviours present different tendencies, we cannot discard that the power

generation effect that we aimed to observe is the reason for the observed behaviours.

In conclusion, we cannot definitely affirm that the effect was observed. More studies would be necessary, including a comparison with the behaviour of similar control junctions, to understand the weight of the presence of the PM particles in these results. Nevertheless, given the deviating behaviours, we might consider that the energy harvesting effect is one of the factors behind the results.

Chapter 5

Conclusions and Future Work

In this thesis, we have studied the physical properties of MTJs containing Ta-doped tunnel barriers, in the scope of trying to reproduce the effect of power generation through the harvesting of thermal fluctuations in paramagnetic centres. Besides that, we also investigated the physics of the underlying mechanisms introduced by the particles, that affect the tunnelling of electrons. Using magnetron sputtering we were able to deposit MgO-based tunnel junctions with TMR ratios over 160% and RxA_P = 3.5 MΩ μm^2, at room temperature. The junctions containing a Ta sub nanolayer presented TMR ratios around 70% and RxA_P = 5.5 MΩ μm^2. Right away, one is able to conclude that the presence of the paramagnetic particles causes an increase in the resistance, which was explained by the increment in the effective thickness due to the introduction of the tantalum particles. At the same time, a lower TMR was observed, due to the opening of extra spin-independent tunnelling paths. These samples showed a strong dependence on both the temperature and bias voltage. Their resistance presented a weak insulator-like behaviour, which shows that part of the transport is achieved through an elastic direct tunnelling mechanism. However, the TMR and the electrical conductance showed to be strongly affected by the increase in voltage and temperature. We have determine that there is an elastic contribution from impurity-assisted tunnelling in the barrier. An inelastic phonon contribution is also considered, due to the ΔG variation with temperature. In order to support our hypothesis, in future work the comparison between the Ta-doped and control junctions will be performed, as a function of temperature, to determine the differences between the V- and T-dependency in a junction with a similar structure.

Concerning the power generation effect, we could not confidently affirm the reproduction of the effect. Several measurements were performed in order to achieve it, and

several studies were carried out with the aim to understand it. Trying to justify the lack of the effect, the first thing we must point out, is the lack of reproducibility associated to it. Since the first record of the observation of the effect, in 2009 [39], only a few publications have been able to reproduce it. In the work developed in Ref. [13], the effect was only detected in 1 out of 200 devices. Given our setup and time limitations, not more than a dozen MTJs were tested. Other than that, one should take in account that this is the first study on the effect of using Ta particles in the tunnel barrier. So, this specific device had never been studied for this application. To obtain a better insight on the parameters that influence the effect, future studies include the fabrication and characterization of devices with varying parameters such as doping concentration, size distribution of the particles, RxA product of the junctions, and thickness of the tunnel barrier. We also aim to perform the comparison of the Ta-doped and control junctions as a function of temperature, to investigate how the observed offsets vary with resistance, with and without the presence of the particles in the barrier.

Bibliography

[1] J. B. Sousa, J. O. Ventura, and A. Pereira, "Chapter 12 - transport at the nanoscale," in *Transport Phenomena in Micro- and Nanoscale Functional Materials and Devices*, ser. Micro and Nano Technologies, J. B. Sousa, J. O. Ventura, and A. Pereira, Eds. William Andrew Publishing, 2021, pp. 363–460. [Online]. Available: https://www.sciencedirect.com/science/article/pii/B9780323460972000069

[2] M. N. Baibich, J. M. Broto, A. Fert, F. N. Van Dau, F. Petroff, P. Etienne, G. Creuzet, A. Friederich, and J. Chazelas, "Giant magnetoresistance of (001)fe/(001)cr magnetic superlattices," *Phys. Rev. Lett.*, vol. 61, pp. 2472–2475, Nov 1988. [Online]. Available: https://link.aps.org/doi/10.1103/PhysRevLett.61.2472

[3] M. Julliere, "Tunneling between ferromagnetic films," *Physics Letters A*, vol. 54, pp. 225–226, 1975.

[4] J. S. Moodera, L. R. Kinder, T. M. Wong, and R. Meservey, "Large magnetoresistance at room temperature in ferromagnetic thin film tunnel junctions," *Phys. Rev. Lett.*, vol. 74, pp. 3273–3276, Apr 1995. [Online]. Available: https://link.aps.org/doi/10.1103/PhysRevLett.74.3273

[5] D. Wang, C. Nordman, J. Daughton, Z. Qian, and J. Fink, "70temperature for sdt sandwich junctions with cofeb as free and reference layers," *IEEE Transactions on Magnetics*, vol. 40, no. 4, pp. 2269–2271, 2004.

[6] "Spintronics: Fundamentals and applications," *Reviews of Modern Physics*, vol. 76, pp. 323–410, 2004.

[7] W. H. Butler, X.-G. Zhang, T. C. Schulthess, and J. M. MacLaren, "Spin-dependent tunneling conductance of Fe|MgO|Fe sandwiches," *Phys. Rev. B*, vol. 63, p. 054416, Jan 2001. [Online]. Available: https://link.aps.org/doi/10.1103/PhysRevB.63.054416

[8] P. Mavropoulos, N. Papanikolaou, and P. H. Dederichs, "Complex band structure and tunneling through ferromagnet /insulator /ferromagnet junctions," *Phys. Rev. Lett.*, vol. 85, pp. 1088–1091, Jul 2000. [Online]. Available: https://link.aps.org/doi/10.1103/PhysRevLett.85.1088

[9] I. I. Oleinik, E. Y. Tsymbal, and D. G. Pettifor, "Structural and electronic properties of Co/al$_2$o$_3$/Co magnetic tunnel junction from first principles," *Phys. Rev. B*, vol. 62, pp. 3952–3959, Aug 2000. [Online]. Available: https://link.aps.org/doi/10.1103/PhysRevB.62.3952

[10] A. M. Bratkovsky, "Assisted tunneling in ferromagnetic junctions and half-metallic oxides," *Applied Physics Letters*, vol. 72, no. 18, pp. 2334–2336, 1998. [Online]. Available: http://link.aip.org/link/?APL/72/2334/1

[11] J. G. Simmons, "Generalized formula for the electric tunnel effect between similar electrodes separated by a thin insulating film," *Journal of Applied Physics*, vol. 34, no. 6, pp. 1793–1803, 1963. [Online]. Available: https://doi.org/10.1063/1.1702682

[12] J. J. Åkerman, R. Escudero, C. Leighton, S. Kim, D. Rabson, R. W. Dave, J. Slaughter, and I. K. Schuller, "Criteria for ferromagnetic–insulator–ferromagnetic tunneling," *Journal of Magnetism and Magnetic Materials*, vol. 240, no. 1, pp. 86–91, 2002, 4th International Symposium on Metallic Multilayers. [Online]. Available: https://www.sciencedirect.com/science/article/pii/S0304885301007120

[13] K. Katcko, E. Urbain, B. Taudul, F. Schleicher, J. Arabski, E. Beaurepaire, B. Vileno, D. Spor, W. Weber, D. Lacour, S. Boukari, M. Hehn, M. Alouani, J. Fransson, and M. Bowen, "Spin-driven electrical power generation at room temperature," *Communications Physics*, vol. 2, 09 2019.

[14] S. Meskine, A. Boukortt, R. Hayn, and A. Zaoui, "Transition between high-spin and low-spin states in mn-doped mgo," *Physica Status Solidi (B) Basic Research*, vol. 251, no. 4, pp. 845–849, 2014.

[15] C. Kittel, *Introduction to Solid State Physics*, 8th ed. Wiley, 2004. [Online]. Available: http://www.amazon.com/Introduction-Solid-Physics-Charles-Kittel/dp/047141526X/ref=dp_ob_title_bk

[16] C. Tiusan, F. Greullet, M. Hehn, F. Montaigne, S. Andrieu, and A. Schuhl, "Spin tunnelling phenomena in single-crystal magnetic tunnel junction systems," *Journal of Physics: Condensed Matter*, vol. 19, no. 16, p. 165201, apr 2007. [Online]. Available: https://doi.org/10.1088/0953-8984/19/16/165201

[17] W. H. Butler, "Tunneling magnetoresistance from a symmetry filtering effect," *Science and Technology of Advanced Materials*, vol. 9, no. 1, p. 014106, jan 2008. [Online]. Available: https://doi.org/10.1088/1468-6996/9/1/014106

[18] H. Wei, Q. Qin, M. Ma, R. Sharif, and X. Han, "80at room temperature for thin al–o barrier magnetic tunnel junction with cofeb as free and reference layers," *Journal of Applied Physics*, vol. 101, pp. 09B501 – 09B501, 06 2007.

[19] S. Ikeda, J. Hayakawa, Y. Ashizawa, Y. Lee, K. Miura, H. Hasegawa, M. Tsunoda, F. Matsukura, and H. Ohno, "Tunnel magnetoresistance of 604suppression of ta diffusion in cofeb/mgo/cofeb pseudo-spin-valves annealed at high temperature," *Applied Physics Letters*, vol. 93, pp. 082 508–082 508, 08 2008.

[20] S. Yuasa and D. D. Djayaprawira, "Giant tunnel magnetoresistance in magnetic tunnel junctions with a crystalline MgO(0 0 1) barrier," *Journal of Physics D: Applied Physics*, vol. 40, no. 21, pp. R337–R354, oct 2007. [Online]. Available: https://doi.org/10.1088/0022-3727/40/21/r01

[21] R. Meservey and P. Tedrow, "Spin-polarized electron tunneling," *Physics Reports*, vol. 238, no. 4, pp. 173–243, 1994. [Online]. Available: https://www.sciencedirect.com/science/article/pii/0370157394901058

[22] Y. Xu, D. Awschalom, and J. Nitta, *Handbook of Spintronics*, 01 2015.

[23] J. M. Teixeira, "Mgo-based magnetic tunnel junctions: Physical studies," Ph.D. dissertation, Faculty of Sciences of the University of Porto, 2010.

[24] S. Zhang, P. M. Levy, A. C. Marley, and S. S. P. Parkin, "Quenching of magnetoresistance by hot electrons in magnetic tunnel junctions," *Phys. Rev. Lett.*, vol. 79, pp. 3744–3747, Nov 1997. [Online]. Available: https://link.aps.org/doi/10.1103/PhysRevLett.79.3744

[25] J. Teixeira, J. Ventura, M. Fernández-García, J. Araujo, j. Sousa, P. Wisniowski, and P. Freitas, "Electrode band structure effects in thin mgo magnetic tunnel junctions," *Applied Physics Letters*, vol. 100, p. 072406, 02 2012.

[26] J. Zhang and R. M. White, "Voltage dependence of magnetoresistance in spin dependent tunneling junctions," *Journal of Applied Physics*, vol. 83, no. 11, pp. 6512–6514, 1998. [Online]. Available: https://doi.org/10.1063/1.367644

[27] G.-X. Miao, K. Chetry, A. Gupta, W. Butler, K. Tsunekawa, D. Djayaprawira, and G. Xiao, "Inelastic tunneling spectroscopy of magnetic tunnel junctions based on cofeb/mgo/cofeb with mg insertion layer," *Journal of Applied Physics*, vol. 99, pp. 08T305 – 08T305, 05 2006.

[28] J. Reiner, S. Cui, Z. Liu, M. Wang, C. Ahn, and T. Ma, "Inelastic electron tunneling spectroscopy study of thin gate dielectrics," *Advanced materials (Deerfield Beach, Fla.)*, vol. 22, pp. 2962–8, 07 2010.

[29] M. Reed, "Inelastic electron tunneling spectroscopy," *Materials Today*, vol. 11, p. 46–50, 11 2008.

[30] A. Vedyayev, D. Bagrets, A. Bagrets, and B. Dieny, "Resonant spin-dependent tunneling in spin-valve junctions in the presence of paramagnetic impurities," *Physical Review B*, vol. 63, no. 6, jan 2001. [Online]. Available: https://doi.org/10.1103%2Fphysrevb.63.064429

[31] X. Kou, J. Schmalhorst, A. Thomas, and G. Reiss, "Temperature dependence of the resistance of magnetic tunnel junctions with mgo barrier," *Applied Physics Letters*, vol. 88, no. 21, p. 212115, 2006. [Online]. Available: https://doi.org/10.1063/1.2206680

[32] H. Kronmüller and S. S. P. Parkin, "Handbook of magnetism and advanced magnetic materials," 2007.

[33] C. H. Shang, J. Nowak, R. Jansen, and J. S. Moodera, "Temperature dependence of magnetoresistance and surface magnetization in ferromagnetic tunnel junctions," *Phys. Rev. B*, vol. 58, pp. R2917–R2920, Aug 1998. [Online]. Available: https://link.aps.org/doi/10.1103/PhysRevB.58.R2917

[34] J. G. Simmons, "Generalized thermal j-v characteristic for the electric tunnel effect," *Journal of Applied Physics*, vol. 35, no. 9, pp. 2655–2658, 1964. [Online]. Available: https://doi.org/10.1063/1.1713820

[35] D. T. Pierce, R. J. Celotta, J. Unguris, and H. C. Siegmann, "Spin-dependent elastic scattering of electrons from a ferromagnetic glass, $ni_{40}fe_{40}b_{20}$," *Phys. Rev. B*, vol. 26, pp. 2566–2574, Sep 1982. [Online]. Available: https://link.aps.org/doi/10.1103/PhysRevB.26.2566

[36] R. Jansen and J. C. Lodder, "Resonant tunneling via spin-polarized barrier states in a magnetic tunnel junction," *Phys. Rev. B*, vol. 61, pp. 5860–5863, Mar 2000. [Online]. Available: https://link.aps.org/doi/10.1103/PhysRevB.61.5860

[37] H. Sukegawa, S. Nakamura, A. Hirohata, N. Tezuka, and K. Inomata, "Significant magnetoresistance enhancement due to a cotunneling process in a double tunnel junction with single discontinuous ferromagnetic layer insertion," *Phys. Rev. Lett.*, vol. 94, p. 068304, Feb 2005. [Online]. Available: https://link.aps.org/doi/10.1103/PhysRevLett.94.068304

[38] F. Guinea, "Spin-flip scattering in magnetic junctions," *Physical Review B*, vol. 58, no. 14, pp. 9212–9216, oct 1998. [Online]. Available: https://doi.org/10.1103%2Fphysrevb.58.9212

[39] P. N. Hai, S. Ohya, M. Tanaka, S. E. Barnes, and S. Maekawa, "Electromotive force and huge magnetoresistance in magnetic tunnel junctions," *Nature*, vol. 458, no. 7237, pp. 489–492, March 2009. [Online]. Available: https://ideas.repec.org/a/nat/nature/v458y2009i7237d10.1038_nature07879.html

[40] G.-X. Miao, J. Chang, B. Assaf, D. Heiman, and J. Moodera, "Spin regulation in composite spin-filter barrier devices," *Nature communications*, vol. 5, p. 3682, 04 2014.

[41] B. Chowrira, L. Kandpal, D. Mertz, C. Kieber, A. Bahouka, R. Bernard, L. Joly, E. Monteblanco, S. Mohapatra, E. Sternitzky, V. da Costa, M. Hehn, F. Montaigne, B. Vileno, F. Choueikani, P. Ohresser, D. Lacour, W. Weber, S. Boukari, and M. Bowen, "Record spintronic harvesting of thermal fluctuations using paramagnetic molecular centers," Nov. 2020, working paper or preprint. [Online]. Available: https://hal.archives-ouvertes.fr/hal-03001215

[42] P. Kelly and R. Arnell, "Magnetron sputtering: a review of recent developments and applications," *Vacuum*, vol. 56, no. 3, pp. 159–172, 2000. [Online]. Available: https://www.sciencedirect.com/science/article/pii/S0042207X9900189X

[43] L. J. Ferreira Martins, "Cofeb/mgo/cofeb-based magnetic tunnel junctions for memory applications: optimization of the fabrication process and magnetic properties," 2016.

[44] J. S. Moodera, J. Nowak, and R. J. M. van de Veerdonk, "Interface magnetism and spin wave scattering in ferromagnet-insulator-ferromagnet tunnel junctions," *Phys. Rev. Lett.*, vol. 80, pp. 2941–2944, Mar 1998. [Online]. Available: https://link.aps.org/doi/10.1103/PhysRevLett.80.2941

[45] T. Dimopoulos, Y. Henry, V. Costa, C. Tiusan, and K. Ounadjela, "Influence of barrier overoxidation and annealing on the inelastic spin-dependent tunneling in alox-based junctions," *Journal of Applied Physics*, vol. 95, pp. 6936–6938, 06 2004.

[46] D. Zhao, Y. Wang, J. Shao, Y. Chen, Z. Fu, Q. Xia, S. Wang, X. Li, G. Dong, M. Zhou, and D. Zhu, "Temperature dependence of tunnel magnetoresistance in serial magnetic tunnel junctions," *AIP Advances*, vol. 12, no. 5, p. 055114, 2022. [Online]. Available: https://doi.org/10.1063/5.0088020

[47] J. Rowell and S. Lundqvist, "Tunnelling phenomena in solids," p. 273, 1969.

[48] V. Drewello, J. Schmalhorst, A. Thomas, and G. Reiss, "Evidence for strong magnon contribution to the tmr temperature dependence in mgo based tunnel junctions," *Phys. Rev. B*, vol. 77, p. 014440, Jan 2008. [Online]. Available: https://link.aps.org/doi/10.1103/PhysRevB.77.014440

[49] R. Jansen and J. S. Moodera, "Magnetoresistance in doped magnetic tunnel junctions: Effect of spin scattering and impurity-assisted transport," *Phys. Rev. B*, vol. 61, pp. 9047–9050, Apr 2000. [Online]. Available: https://link.aps.org/doi/10.1103/PhysRevB.61.9047

[50] C. H. de Groot, Y. Ouyang, S.-M. Koo, E. Kendall, Q. Q. Shu, and J. S. Moodera, "Resonant tunnelling in dy- or gd-doped al2o3 magnetic tunnel junctions," *Journal of Physics: Condensed Matter*, vol. 14, no. 20, pp. 5153–5159, may 2002. [Online]. Available: https://doi.org/10.1088/0953-8984/14/20/310

[51] J. Moodera, T.-H. Kim, C. Tanaka, and C. de Groot, "Spin-polarized tunneling, magnetoresistance and interfacial effects in ferromagnetic junctions," *Phil. Mag. B*, vol. 80, p. 195, 2000. [Online]. Available: https://eprints.soton.ac.uk/257457/

[52] E. Y. Tsymbal and D. G. Pettifor, "The influence of impurities within the barrier on tunneling magnetoresistance," *Journal of Applied Physics*, vol. 85, no. 8, pp. 5801–5803, 1999. [Online]. Available: https://doi.org/10.1063/1.369924

[53] R. Meservey, P. M. Tedrow, and J. S. Brooks, "Tunneling characteristics of amorphous si barriers," *Journal of Applied Physics*, vol. 53, no. 3, pp. 1563–1570, 1982. [Online]. Available: https://doi.org/10.1063/1.330658